

# Image Quality Assessment: From Human to Machine Preference

Chunyi Li<sup>1,2,4\*</sup>, Yuan Tian<sup>1,2\*</sup>, Xiaoyue Ling<sup>1\*</sup>, Zicheng Zhang<sup>1,2</sup>, Haodong Duan<sup>2</sup>, Haoning Wu<sup>3,4</sup>,  
Ziheng Jia<sup>1</sup>, Xiaohong Liu<sup>1</sup>, Xionguo Min<sup>1</sup>, Guo Lu<sup>1†</sup>, Weisi Lin<sup>4</sup>, Guangtao Zhai<sup>1,2†</sup>  
Shanghai Jiao Tong University<sup>1</sup>, Shanghai AI Lab<sup>2</sup>, Moonshot AI<sup>3</sup>, Nanyang Technological University<sup>4</sup>

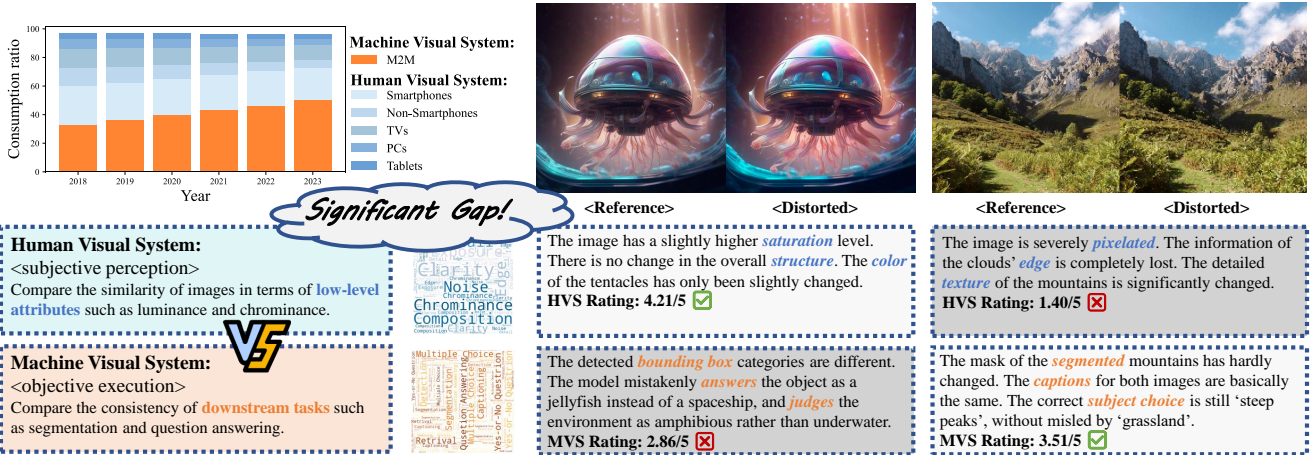


Figure 1. The significant gap between the well-explored **Human Vision System (HVS)** and the emerging **Machine Vision System (MVS)**. Their different perception mechanisms leading to images that are subjectively satisfactory to humans not being applicable to the machines downstream tasks such as detection and question answering, vice versa.

## Abstract

*Image Quality Assessment (IQA) based on human subjective preferences has undergone extensive research in the past decades. However, with the development of communication protocols, the visual data consumption volume of machines has gradually surpassed that of humans. For machines, the preference depends on downstream tasks such as segmentation and detection, rather than visual appeal. Considering the huge gap between human and machine visual systems, this paper proposes the topic: **Image Quality Assessment for Machine Vision** for the first time. Specifically, we (1) defined the subjective preferences of machines, including downstream tasks, test models, and evaluation metrics; (2) established the Machine Preference Database (MPD), which contains 2.25M fine-grained annotations and 30k reference/distorted image pair instances; (3) verified the performance of mainstream IQA algorithms on MPD. Experiments show that current IQA metrics are human-centric and cannot accurately characterize machine preferences. We sincerely hope that MPD can promote the evolution of IQA from human to machine preferences. Project page is on: <https://github.com/lcysyxdxc/MPD>.*

\* Equal contribution. † Corresponding authors.

## 1. Introduction

The rapid ascend of smart cities [20] and the flourishing of the Internet of Things (IoT) [86] over the past decade have fundamentally transformed the framework of the application end. According to the Cisco [13] white paper, the number of Machine-to-Machine (M2M) connections first exceeded that of Machine-to-Human (M2H) in 2023, reaching 147 billion. Machines have gradually replaced humans and become the primary consumers of image/video data. In the field of image processing, the primary goal is to enhance the quality of processed images, ensuring they conform to human perception. Previously, the performance of a compression/reconstruction/generation algorithm [39–41] is often judged by its visual appeal to humans. This technology, known as Image Quality Assessment (IQA), comprehensively models the Human Visual System (HVS) to predict human subjective preferences. Consequently, with the evolution of application ends, IQA today has to transcend HVS and serve Machine Vision Systems (MVS) more effectively.

However, there are significant disparities in the perceptual mechanisms between HVS and MVS. This discrepancy arises because HVS prioritizes the similarity between reference and distorted images, such as texture, structure, and color, whereas machines focus on the consistency of results

Table 1. Comparison of MPD with other IQA databases. As the first machine preference-oriented library, MPD has a larger image scale, a wider range of corruption scenarios, and more complete annotation content.

Database	Image			Corruption		Annotation		
	Reference	Distorted	Resolution	Types	Strength	Num	Dimension	Labeling Criteria
LIVE[57]	29	779	768	5	5	25k	1	Human preference on NSIs
TID2013[61]	25	3k	512	24	5	514k	1	Human preference on NSIs
KADID-10K[47]	81	10k	1k	25	5	304k	1	Human preference on NSIs
CLIC2021[6]	585	3k	1k	10	3	484k	1	Human preference on compressed images
NTIRE2022[24]	250	29k	288	40	5	1.13m	1	Human preference on super-resolution images
KonIQ-10K[29]	-	10k	1k	-	-	1.21m	5	Human preference on NSIs
AGIQA-3K[35]	-	3k	1k	-	-	125k	2	Human preference on AIGIs
NTIRE2024[38]	-	20k	1k	-	-	420k	2	Human preference on AIGIs
<b>MPD (ours)</b>	<b>1k</b>	<b>30k</b>	<b>1k</b>	<b>30</b>	<b>5</b>	<b>2.25m</b>	<b>5</b>	<b>Machine preference on NSIs, SCIs, and AIGIs</b>

in downstream tasks. As illustrated in Figure 1, for distortions resulting from factors like encoding/quantization, HVSs perceive a noticeable degradation in quality, yet the performance of tasks like segmentation/detection by machines remains unaffected. Conversely, some minor disturbances that the human eye barely notices can significantly disrupt the output of MVSs, making it difficult to migrate their evaluation algorithms.

What images do machines prefer? This remains an open question. For HVS, over the past two decades, IQA has witnessed significant development. Given the variations in image preferences among individuals, particularly across dimensions such as brightness and chroma, the scoring dimensions, the annotations from multiple subjects, and the integration of these annotations into global subjective preference labels have been well established. Hundreds of fine-grained databases can drive IQA algorithms that closely align with human perception. Conversely, MVS development is much slower, regardless of an end-to-end IQA algorithm, there is even no database that annotates images with an overall preference score of machines. This hinders the comprehensive evaluation of image processing metrics designed for machine vision, limiting the experience of application ends. Considering these issues, we first attempt to generalize the concept of IQA from HVS to MVS. Our contributions can be summarized as follows:

- A innovative definition of the subjective preferences of machines. We propose a standardized process for collecting subjective labels from machines. Specifically, we identify the downstream tasks that determine the quality of machine perception, including four multimodal tasks related to Large Multimodal Models (LMMs) and three classic Computer Vision (CV) tasks. By referencing the multi-dimensional scoring mechanism of humans, we comprehensively evaluate the performance of machines in these tasks to obtain ground truth labels.
- A large-scale database named the Machine Preference Database (MPD). Using 15 general LMMs and 15 spe-

cialized CV models, we collected 2.25 million preference data points on 30,000 reference/distorted image pairs, establishing the first IQA database for machine vision. In particular, we conducted an in-depth analysis of each participating machine to explore the internal patterns of MVS perception and their differences with HVS.

- A complex benchmark test for existing IQA algorithms. Experiments on the MPD demonstrate that these algorithms designed for HVS cannot fully model MVS, whose predictions do not match machine ratings. After fine-tuning based on the MPD, their performance improves slightly, but still cannot characterize machine preferences, especially when facing mild distortion.

## 2. Related Works

### 2.1. Image Quality Assessment Database

IQA datasets include Full Reference (FR) and No Reference (NR). FR datasets manually add corruption to reference images, whereas NR directly capture distorted images. Typically, these datasets focus on a single image type, such as Natural Scenes Images (NSIs) [6, 24, 47, 57, 61], Screen Content Images (SCIs) [21, 56, 58], and AI-Generated Images (AIGIs) [35, 38, 51, 91], with quality labels derived solely from human preferences as listed in Table 1. On contrast, in the era where machines surpass humans as application ends, MPD stands out as the first machine preference-oriented library. It offers a larger image scale, a broader range of corruption scenarios, and a more comprehensive annotation context than other IQA databases.

### 2.2. Machine Vision Downstream Task

In the absence of a unified quality indicator, image processing algorithms, taking compression and restoration metrics for machine vision for example, are often in a fragmented state, with the performance of each algorithm being validated by only one or two downstream tasks. [93, 94] These tasks vary, as do the models used to perform them, mak-

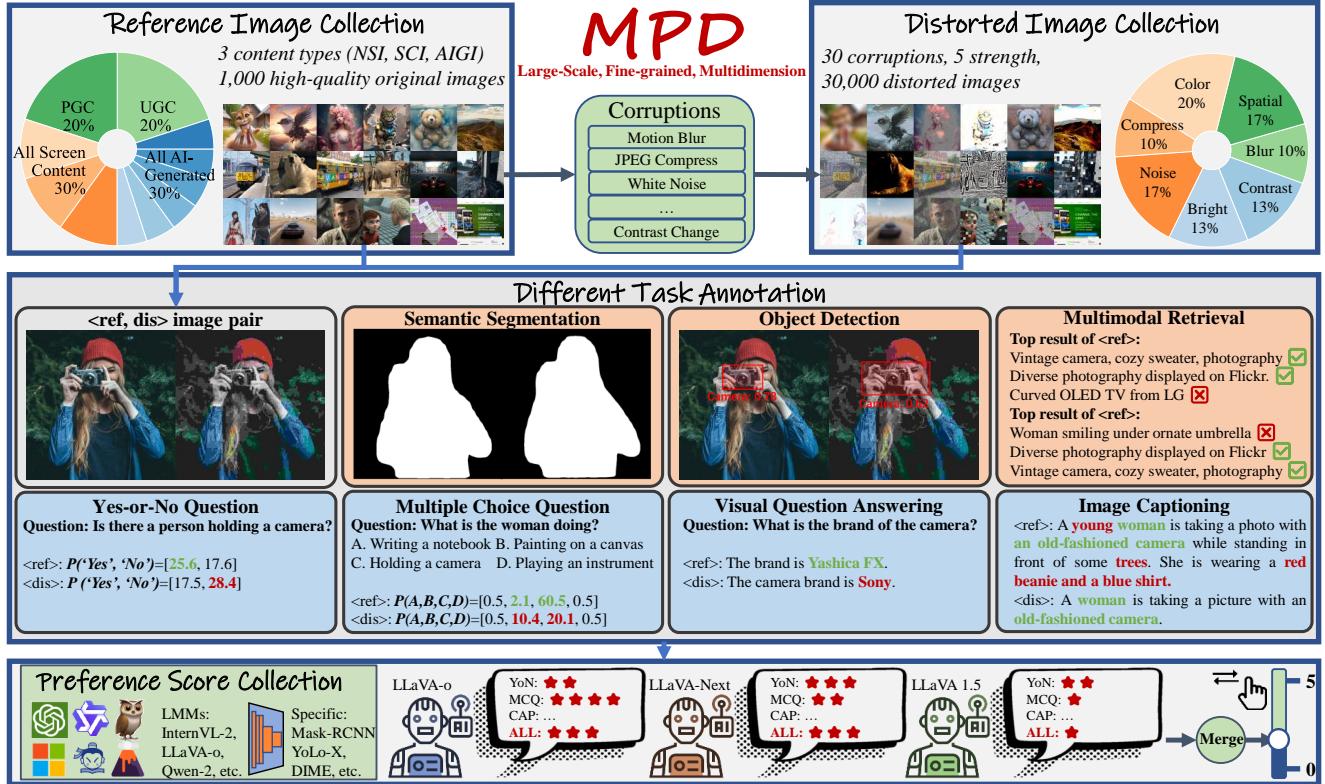


Figure 2. Overview of Machine Preference Database (MPD), with 30k large-scale reference/distorted image pairs, meticulously annotated with 2.25M fine-grained preference score from the mean opinion of 15 mainstream LLMs and 15 specific CV models. It provides a multi-dimensional fidelity evaluation of various downstream machine vision tasks.

ing the evaluation criteria disparate and incomplete. For compression algorithms, validation indicators include the classification [30, 60], image captioning [12], object detection [80], or semantic segmentation [31] result before/after compression, with each indicator differing and lacking standardization or completeness. Restoration algorithms fare slightly better, with most consistently relying on object detection [48, 83, 84]. Nevertheless, some employ traditional Fast-RCNN [65], while others utilize more advanced models like ViTDet[34]. The variation in model bases further compromises the comprehensiveness and objectivity of the evaluation outcomes. Thus, there is an urgent need for a unified representation of machine preferences.

### 3. Database Construction

#### 3.1. Reference & Distorted Image Collection

Similar to the previous IQA database, we first selected 1,000 high-quality reference images and then artificially degraded their quality to obtain 30,000 pairs of reference and distorted images. To comprehensively represent the common content on the internet, we referred to the CMC-Bench [42] and selected the three most common image categories: Natural Scene Images (NSIs), including

User/Professional Generated Content (UGC/PGC) [6, 46]; Screen Content Images (SCIs), including webpages [67], games [92], and movies [56]; and AI-Generated Images (AIGIs), generated by six representative text-to-image models [8, 25, 28, 43, 64, 66]. The collection process is shown in Figure 2. Both human viewers and IQA models have verified this image sequence to ensure that they are undistorted as reference images.

For the distorted images, we modeled the corruption caused by the current communication protocols, which were divided into 30 scenarios. Specifically, these corruptions were classified into seven categories: Blur, various types of unclear image; Luminance, global brightness changes; Chrominance, global color changes; Contrast, global changes in contrast/saturation; Noise, random noise of different distributions; Compression, codec algorithm like JPEG; and Spatial, local pixel-level changes.<sup>1</sup> For each corruption, we defined five levels of intensity, from mild to severe. To fairly explore the impact of each corruption, we artificially control the distortion strength to ensure that quality degradation perceived by the human eye is

<sup>1</sup>For the definition of all these 30 corruptions, specific details, and examples, please refer to the appendix.

aligned at the same level. Thus, for each reference image, we randomly selected the intensity to add all the corruptions mentioned above, resulting in 30,000 distorted images. The reference/distorted image pairs will then be annotated by machine subjects.

### 3.2. Different Task Annotation

In the past five years, the evaluation of image processing algorithms for machine vision has primarily focused on seven tasks: Regression, Classification, Visual Question Answering (VQA), Caption (CAP), Segmentation (SEG), Detection (DET), and Retrieval (RET). Among these, the first four tasks can be accomplished by general LMMs, whereas the latter three tasks necessitate specialized models due to their unique requirements. Note that the regression and classification tasks in this context are analogous to Yes-or-No (YoN) and Multiple-Choice Questions (MCQ) within LMMs. To this end, we enlisted five experienced human experts to design YoN/VQA/CAP questions and answers for 1,000 reference images. These questions are designed to be challenging, as illustrated in the example provided in Figure 2, especially in the MCQ sets where confusion options are introduced. This approach enables us to accurately measure the degree of quality degradation perceived by the machine.

We apply these seven tasks to both the reference and distorted images, measure the similarity of the output results, and derive scores for each of the seven sub-dimensions. Specifically, for **YoN** tasks, we employ a logit-level evaluation approach based on softmax similarity, as previous LMM benchmarks [50, 78] do. This entails LMMs confirming or denying the questions designed for each reference/distorted image pair. The confidence difference in the next token output, 'Yes' or 'No', reflects the difference in the perceptual quality degradation from the perspective of machines, namely a score  $S_{YoN}$ :

$$S_{YoN} = |\sigma(P_{dis}(\text{Yes}, \text{No})) - \sigma(P_{ref}(\text{Yes}, \text{No}))|, \quad (1)$$

where  $P_{dis,ref}(\cdot)$  denotes the output probability of certain logits, normalized by the softmax function  $\sigma(\cdot)$ . **MCQ** tasks follow a similar evaluation paradigm. We set a correct option and three confusing options (the options are usually no more than 4, see [18, 50, 79]), and the model outputs the probability of each option as a four-element vector. The distance between the two vectors in space can reflect the perceptual quality score  $S_{MCQ}$  for machines:

$$S_{MCQ} = \cos(P_{dis}(A, B, C, D), P_{ref}(A, B, C, D)), \quad (2)$$

where the distance is measured by cosine similarity. For **VQA** tasks, we conduct sentence-level evaluation beyond the logits. LMMs will be required to answer a certain question in about 5 words, and the semantic difference between two output sentences will be the score  $S_{VQA}$ :

$$S_{VQA} = \text{CLIP}(T_{dis}, T_{ref}), \quad (3)$$

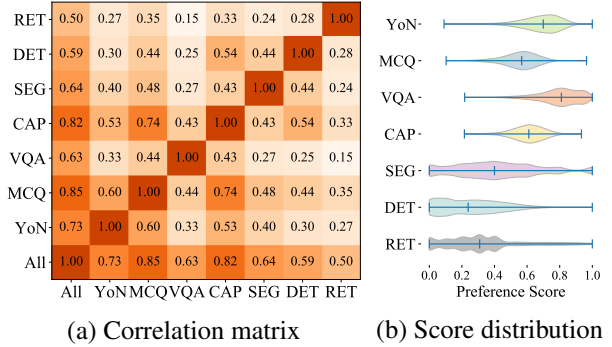


Figure 3. Correlation between the general preference score and the score in seven different downstream tasks.

where  $T_{dis,ref}$  represents the whole output text, measured by the CLIP text encoder. **CAP** tasks require a longer output, by describing the main subjects, actions, settings, and any notable objects or features of the image in about 40 words. Considering the remarkable text length, we use indicators dedicated to image captioning to analyze the differences between the two long sentences in  $S_{CAP}$ :

$$S_{CAP} = \sum_{eval} \text{eval}(T_{dis}, T_{ref}), \quad (4)$$

where  $eval \in (\text{BLEU}, \text{CIDEr}, \text{SPICE})$  [4, 59, 72], three most commonly-used captioning indicators. Then, for **SEG** tasks, referring to their common evaluation criteria [26], we calculate the Intersection-over-Union (IoU) ratio in  $S_{SEG}$ :

$$S_{SEG} = \text{IoU}(M_{dis}, M_{ref}), \quad (5)$$

where  $M_{dis,ref}$  stands for binarized segmentation masks. **DET** tasks will be more complex, whose results include both spatial information and category labels. Thus, we consider the detection failed when the categories are different, and only further calculate the IoU when they are consistent [96], as described in  $S_{DET}$ :

$$S_{DET} = \text{Acc}_1(C_{dis}, C_{ref}) \cdot \text{IoU}(B_{dis}, B_{ref}), \quad (6)$$

where  $C_{dis,ref}$  denotes the category sequence ordered by confidence, and  $B_{dis,ref}$  is the detected bounding box. Finally for **RET** tasks, we merge three common Image-to-Text retrieval indicators [7], namely Top-1/5/10 accuracy, to evaluate the retrieved sequence as  $S_{RET}$ :

$$S_{RET} = \sum_{i \in \{1, 5, 10\}} \text{Acc}_i(C_{dis}, C_{ref}). \quad (7)$$

After the above process, we can obtain the preferences of LMMs in the first four dimensions, and the preferences of each specific CV model on its target task.

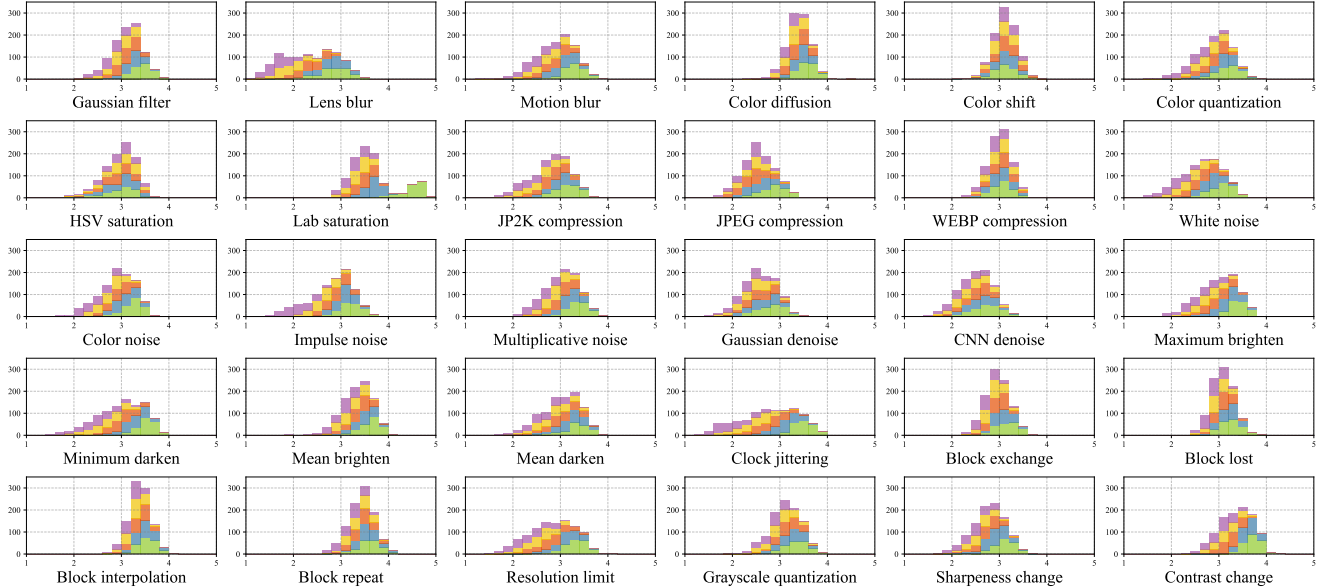


Figure 4. MOS score of MPD, visualized in 30 corruption subsets. Different color denotes corruption strength **Level 1-Level 2-Level 3-Level 4-Level 5**. Results show the sensitivity of the machines to each corruption varied significantly.

### 3.3. Preference Score Collection

Following the ITU human subjective annotation standards [71], we adopt the same settings to obtain the machine Mean Opinion Score (MOS). Specifically, for YoN, MCQ, VQA, and CAP tasks, we use 15 general LMMs for inference, namely DeepseekVL [53], InstructBLIP [14], InternVL2 [11], InternLM-XComposer2 [16], LLaVA1.5 [49], LLaVAnext [44], LLaVA-OneVision [37], Mantis [32], MiniInternVL [22], MPlugOwl3 [81], Ovis [54], Phi3.5 [1], Pangea [85], Qwen2-VL [75], and Yi1.5 [52]. We set all temperature parameters as 0 to avoid unstable output to ensure all perceptual quality degradations come from distortion. Comprehensively considering popular trends and performance, we implement 5 models for each specific CV tasks, namely SEG: BoxInst [70], ConvNext [77], Mask-RCNN [27], SCNet [73], and RTMDet (segmentation mode) [55]; DET: Dino[89], Mask-RCNN [65], RTMDet (detection mode) [55], ViTDet [34], and Yolo-X [23]; RET: DIME [63], InternVL (retrieval-based tuning) [10], LAVIS (retrieval-based tuning) [36], NAAF [90], and VSE++ [19]. After obtaining scores for these 7 tasks, the evaluation can be divided into five dimensions, one dimension for each first four LMM tasks, and the last three tasks are unified into the last dimension, ensuring 15 subjects in each (0, 1) score for MOS. Thus merging all five dimensions into the (0, 5) MOS. Note that we normalize the score of each dimension to avoid where one dimension has a higher score while another is lower (e.g. VQA/CAP), which would lead to unfairness in the weight of the overall MOS.

In addition, considering the rapid development of LMM, we also apply 3 advanced LMMs, GPT4o [2], GPT4o-

mini [2], InternLM-XComposer2d5 [16]; and 4 early-stage LMMs, QWen1.5-VL [5], VisualGLM [17], Monkey [45], MPlugOwl2 [82] on certain tasks. We compared these results with the above-mentioned data in MPD, to prove the long-term usability of MPD through their consistency.

### 4. Database Validation

This section analyzes the preference data characteristics of MPD, to prove the usability of this database, including two perspectives: (1) the mean opinion of all machines; (2) the difference between each machine as a subject.

**Overall:** The MOS of MPD and the sub-scores of the seven tasks are illustrated in Figure 3, with their correlation quantified by Spearman Rank-order Correlation Coefficient (SRCC). Notably, the inter-task correlation is relatively low, particularly for VQA and the three tasks that rely on specialized CV models. Given the current state of image processing algorithms for machine vision, each employing different tasks as performance metrics, the universality and robustness of such evaluation are inherently constrained. The data distribution further substantiates this argument, with YoN/MCQ/CAP being more evenly distributed, VQA exhibiting a higher concentration of high scores, and SEG/DET/RET clustering at lower scores. Moreover, the strong correlation between the total score and the other tasks is evident, with all SRCC surpassing 0.5, underscoring the reliability of the MPD, for various downstream tasks. The MOS distribution across 30 types of corruption and 5 strength levels is depicted in Figure 4. Results show for corruption scenarios that appear similar to HVS, the MVS perception mechanism diverges significantly. For

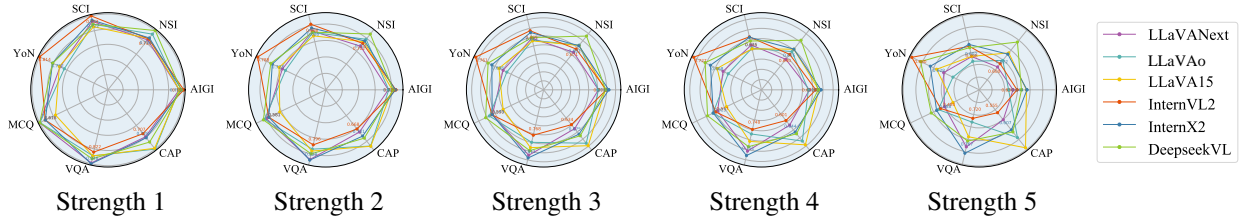


Figure 5. Annotations from different LMMs subjects in MPD under 5 corruption strengths, including 3 content types and 4 tasks.

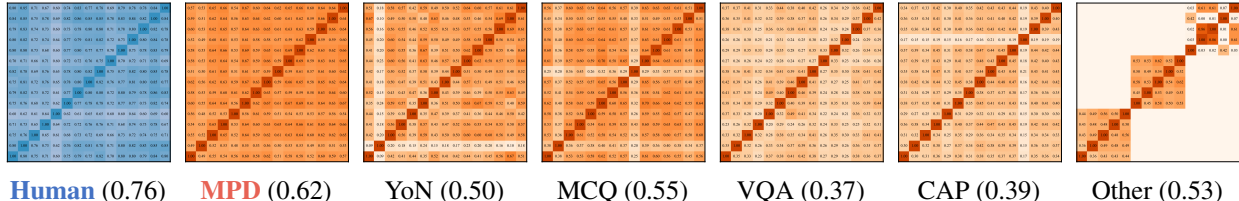


Figure 6. Correlation matrix of the proposed MPD in each dimension. A darker color denotes a higher SRCC, with mean SRCC attached below each matrix. The index of each matrix is arranged in the  $\uparrow, \rightarrow$  directions, in the same order as Section 3.3. The correlation between **human** subjects is greater than **machines**, and the correlation of the overall MOS is greater than the score in each dimension.

instance, the machine is highly sensitive to ‘Lens blur’ but rarely affected by ‘Mean brighten’. A typical example is the four Macro Block-related corruptions, which are nearly indistinguishable for HVS but exhibit significantly lower perception quality for MVS when encountering ‘Block exchange’ compared to the other three. Furthermore, the impact of distortion intensity on the MVS perceptual quality varies markedly. For example, as the intensity level increases, the ‘Lab saturation’ quality diminishes, while the ‘HSV saturation’ quality remains unchanged. These findings underscore the differences between MVS and HVS, reinforcing the significance of establishing such a unified quality representation in MPD.

**Each machine:** We visualize the benchmark performance of six typical LMMs (as space limited) under different corruption strengths, as shown in Figure 5. For different content types, the scores of various machines on NSI/SCI/AIGI dimensions do not vary significantly. For different tasks, advanced models such as InternVL2 excel in dealing with distorted images in YoN, while traditional models like LLaVA1.5 can provide relatively stable results in CAP. As the corruption strength increases by one level, the scores of each dimension decrease by 0.01-0.02. Finally, for all machine subjects, we explored their internal differences in Figure 6. We manually conducted human annotation for 500 instances (the same 15 subjects) and compared the preference differences between humans and machines. The index of each matrix (i.e., the machine it represents) is arranged in the  $\uparrow$  and  $\rightarrow$  directions, in the same order as in Section 3.3. Overall, the SRCC between humans is 0.76, while that of machines is only 0.62, indicating that the divergence in machine image preferences is greater than that of humans. Further exploration of the preference scores

for each dimension shows that the relatedness of machines in VQA and CAP tasks is the lowest. Additionally, there are a few subjects whose assessments differ significantly from other machines<sup>2</sup>, such as InstructBlip in YoN, Mantis in MCQ, Pangea in CAP, and DIME/NAAF in RET. This is often due to special token outputs or multilingual mechanisms, which lead to insufficient robustness, resulting in a higher proportion of errors in distorted images compared to other models, thus leading to inconsistent results. In summary, the larger preference differences make IQA for MVS a more difficult problem than traditional IQA, but also a more valuable and promising research topic.

## 5. Experiment

### 5.1. Experiment Setups

We randomly partitioned the MPD into the train/val set, with 24,000 and 6,000 reference and distorted image pairs, respectively, according to an 8:2 ratio. For MVS, Figure 4 illustrates significant variations in the perceptual quality of different corruptions. Given that machines exhibit a larger Just Noticeable Difference (JND) than humans, our corruption strength exceeds that of previous IQA databases for humans<sup>3</sup>. To conduct a realistic and reliable evaluation of machine preference, we designate the val set as ‘Severe Distortion’ and select a subset of ‘Mild Distortion’ to represent the corruption strength in the real world. The specific splitting

<sup>2</sup>The ITU human subjective annotation standard [71] for humans will exclude data with weak correlation with other subjects, but this is to prevent eye fatigue or malicious attacks during annotation. Given that the machine’s inference process is completely objective, we will refer to the outputs of each machine rather than excluding them.

<sup>3</sup>See appendix for visualization in 5 corruption strength, where the Level 1 of our MPD can even ensemble Level 4 in KADID-10K[47].

Table 2. Using IQA metrics to predict machine preference, including baseline, FR, and NR algorithm, human visual system-based metrics are marked in  $\heartsuit$ . The first row represents two distortion intensities and three image content subsets, and the second row represents five scoring dimensions. [Keys: **Best**; **Second best**; **Baseline (BL)**; Inferior to the baseline.]

Type	Metric	HVS	Severe Distortion			Mild Distortion			NSI			SCI			AIGI		
			SRCC $\uparrow$	KRCC $\uparrow$	PLCC $\uparrow$	SRCC $\uparrow$	KRCC $\uparrow$	PLCC $\uparrow$	SRCC $\uparrow$	KRCC $\uparrow$	PLCC $\uparrow$	SRCC $\uparrow$	KRCC $\uparrow$	PLCC $\uparrow$	SRCC $\uparrow$	KRCC $\uparrow$	PLCC $\uparrow$
BL	PSNR		0.3873	0.2672	0.4664	<b>0.3097</b>	<b>0.2127</b>	<b>0.6197</b>	0.4116	0.2820	0.4945	0.3135	0.2146	0.3329	0.5225	0.3684	<b>0.5985</b>
	SSIM[76]		<b>0.5969</b>	<b>0.4157</b>	<b>0.5537</b>	0.2672	0.1828	0.2818	<b>0.6288</b>	<b>0.4466</b>	<b>0.5932</b>	<b>0.5415</b>	<b>0.3748</b>	<b>0.5393</b>	<b>0.5980</b>	<b>0.4278</b>	0.5687
FR	AHIQ[33]		0.8061	0.6153	<b>0.8183</b>	<b>0.5304</b>	<b>0.3685</b>	<b>0.5111</b>	0.8447	0.6601	<b>0.8502</b>	0.7962	0.6040	<b>0.8470</b>	0.7996	0.6082	<b>0.7966</b>
	CKDN[95]	$\heartsuit$	0.7484	0.5560	0.7174	0.0604	0.0405	0.1061	0.8100	0.5988	0.7670	0.7203	0.5171	0.7661	0.6992	0.5102	0.6869
	DISTS[15]		0.7381	0.5443	0.7372	0.4616	0.3232	0.4486	0.7912	0.6060	0.8046	0.7275	0.5384	0.7429	0.7219	0.5365	0.7292
	LPIPS[87]	$\heartsuit$	0.6253	<b>0.4455</b>	0.5601	0.0079	0.0092	0.0056	0.6965	0.5132	0.6478	0.5618	0.3920	0.5686	0.6429	0.4518	<b>0.5481</b>
	PieAPP[62]	$\heartsuit$	<b>0.4737</b>	0.0163	<b>0.2377</b>	0.3030	0.2100	0.2349	0.4536	0.1187	<b>0.2729</b>	0.5173	<b>0.0954</b>	<b>0.2135</b>	<b>0.4614</b>	<b>0.2009</b>	0.3168
	TOPIQ-FR[9]	$\heartsuit$	0.7178	0.5252	0.7182	0.4248	0.2944	<b>0.4841</b>	0.7506	0.5614	0.7585	0.7243	0.5322	0.7186	0.6943	0.5063	0.7061
NR	ARNIQA[3]		<b>0.8337</b>	<b>0.6426</b>	<b>0.8112</b>	0.2388	0.1608	0.2754	<b>0.8704</b>	<b>0.6690</b>	0.8478	<b>0.8220</b>	<b>0.6217</b>	0.8420	<b>0.8449</b>	<b>0.6578</b>	0.7954
	CLIPQA[74]	$\heartsuit$	0.6498	0.4662	0.5901	0.1822	0.1210	0.1797	0.7670	0.5771	0.7141	0.6690	0.4751	0.6215	0.6877	0.4934	0.5977
	DBCNN[88]	$\heartsuit$	<b>0.5652</b>	<b>0.3908</b>	0.5696	0.1334	0.0894	0.1594	0.5978	0.4181	0.6219	0.5692	0.3974	0.6092	<b>0.5422</b>	0.3810	<b>0.5613</b>
	HyperIQA[68]		<b>0.8105</b>	<b>0.6189</b>	0.8012	<b>0.5388</b>	<b>0.3774</b>	0.4712	<b>0.8908</b>	<b>0.7074</b>	<b>0.8691</b>	<b>0.8273</b>	<b>0.6403</b>	<b>0.8601</b>	<b>0.8212</b>	<b>0.6242</b>	<b>0.8076</b>
	NIMA[69]		0.7562	0.5657	0.7858	0.4570	0.3171	0.4342	0.8153	0.6203	0.8224	0.7800	0.5881	0.8092	0.7846	0.5953	0.7622
	TOPIQ-NR[9]	$\heartsuit$	0.6562	0.4616	0.6358	0.1961	0.1318	0.1989	0.7011	0.4823	0.6613	0.6645	0.4624	0.6353	<b>0.5461</b>	<b>0.3422</b>	0.5249
Type	Metric	HVS	YoN			MCQ			VQA			CAP			Others		
			SRCC $\uparrow$	KRCC $\uparrow$	PLCC $\uparrow$	SRCC $\uparrow$	KRCC $\uparrow$	PLCC $\uparrow$	SRCC $\uparrow$	KRCC $\uparrow$	PLCC $\uparrow$	SRCC $\uparrow$	KRCC $\uparrow$	PLCC $\uparrow$	SRCC $\uparrow$	KRCC $\uparrow$	PLCC $\uparrow$
BL	PSNR		0.2753	0.1892	0.3467	0.3273	0.2239	0.4372	0.2067	0.1378	0.2120	0.4319	0.2993	0.4989	0.3798	0.2617	0.4683
	SSIM[76]		<b>0.3960</b>	<b>0.2728</b>	<b>0.3804</b>	<b>0.5089</b>	<b>0.3499</b>	<b>0.4880</b>	<b>0.2960</b>	<b>0.1988</b>	<b>0.2756</b>	<b>0.5550</b>	<b>0.3861</b>	<b>0.5447</b>	<b>0.5072</b>	<b>0.3491</b>	<b>0.4766</b>
FR	AHIQ[33]		<b>0.6017</b>	<b>0.4283</b>	<b>0.6212</b>	<b>0.7314</b>	<b>0.5374</b>	<b>0.7466</b>	0.4244	0.2924	<b>0.4583</b>	<b>0.7220</b>	<b>0.5341</b>	<b>0.7546</b>	0.6184	0.4396	0.6311
	CKDN[95]	$\heartsuit$	0.5491	0.3799	0.5482	0.6866	0.4863	0.6596	0.4045	0.2763	0.3900	0.7044	0.5136	0.6991	0.5434	0.3822	0.5313
	DISTS[15]		0.5267	0.3695	0.5394	0.6486	0.4625	0.6549	0.3512	0.2395	0.3676	0.6649	0.4833	0.6812	0.6203	0.4419	<b>0.6332</b>
	LPIPS[87]	$\heartsuit$	0.4677	0.3252	0.4245	0.5517	0.3912	0.5169	0.3216	0.2169	0.2935	0.5620	0.3996	0.5473	<b>0.4927</b>	<b>0.3387</b>	<b>0.4242</b>
	PieAPP[62]	$\heartsuit$	<b>0.3308</b>	<b>0.0173</b>	<b>0.1663</b>	<b>0.4310</b>	<b>0.1900</b>	<b>0.2087</b>	<b>0.2385</b>	<b>0.0132</b>	<b>0.1032</b>	<b>0.4220</b>	<b>0.0152</b>	0.2136	<b>0.3735</b>	<b>0.0209</b>	<b>0.1747</b>
	TOPIQ-FR[9]	$\heartsuit$	0.5011	0.3480	0.5118	0.6038	0.4232	0.6165	0.3700	0.2508	0.3899	0.6327	0.4545	0.6479	0.6199	0.4383	0.6281
NR	ARNIQA[3]		<b>0.6228</b>	<b>0.4394</b>	<b>0.6172</b>	<b>0.7342</b>	<b>0.5351</b>	<b>0.7242</b>	<b>0.4409</b>	<b>0.3026</b>	0.4454	<b>0.7656</b>	<b>0.5693</b>	<b>0.7664</b>	<b>0.6560</b>	<b>0.4566</b>	0.6309
	CLIPQA[74]	$\heartsuit$	0.4613	0.3167	0.4386	0.5090	0.3556	0.5117	0.2971	0.2028	0.3204	0.6379	0.4551	0.5673	0.5751	0.4048	0.4747
	DBCNN[88]	$\heartsuit$	<b>0.3798</b>	<b>0.2567</b>	0.3969	<b>0.4793</b>	<b>0.3258</b>	0.4951	<b>0.2556</b>	<b>0.1719</b>	0.2783	<b>0.5240</b>	<b>0.3633</b>	<b>0.5388</b>	0.5085	<b>0.3465</b>	0.5093
	HyperIQA[68]		0.6010	0.4278	0.6066	0.7066	0.5155	0.7146	0.4322	0.2996	0.4419	0.7153	0.5234	0.7443	<b>0.6461</b>	<b>0.4598</b>	<b>0.6329</b>
	NIMA[69]		0.5544	0.3904	0.5887	0.6893	0.5002	0.7036	<b>0.4460</b>	<b>0.3074</b>	<b>0.4775</b>	0.6313	0.4531	0.6842	0.5810	0.4106	0.6181
	TOPIQ-NR[9]	$\heartsuit$	0.4939	0.3358	0.4797	0.5469	0.3713	0.5370	0.3578	0.2437	0.3787	<b>0.5112</b>	<b>0.3375</b>	<b>0.5089</b>	0.5769	0.3934	0.5564

mechanism is detailed in the Appendix. To benchmark the performance of quality metrics, three global indicators were employed: SRCC, Kendall Rank-order Correlation Coefficient (KRCC), and Pearson Linear Correlation Coefficient (PLCC), to evaluate the consistency between the objective quality score and the subjective MOS. Among these, SRCC and KRCC represent the prediction monotonicity, while PLCC measures the accuracy.

12 mainstream IQA metrics are implemented for comparison, which have all shown satisfying results in previous human-centric IQA tasks, including 6 FR metrics: AHIQ [33], CKDN [95], DISTS [15], LPIPS [87], PieAPP [62], TOPIQ-FR [9]; and 6 NR metrics: ARNIQA [3], CLIPQA [74], DBCNN [88], HyperIQA [68], NIMA [69], TOPIQ-NR [9]. Some methods specifically model the HVS, such as DBCNN, which has a dedicated stage for simulating human perception; others rely on the remarkable fitting ability of large-scale parameters, like the ViT in AHIQ. We have marked all HVS-based metrics as  $\heartsuit$ . Moreover, two naive quality indicators, PSNR and SSIM [76] are set as the baseline. We train the above 12 metrics on MPD with the learning rate as  $10^{-5}$  for 50 epochs, under the default settings in pyiqa [9] toolbox and evaluate the performance on

the two subsets above, three content types, and five scoring dimensions. We collect MPD preference annotations on  $16 \times$  NVIDIA A800 SXM4 80GB GPUs, and then conduct IQA training/validation on one GPU above.

## 5.2. Experiment Result and Discussion

Table 2 presents the performance of current advanced IQA models on the MPD. Overall, regardless of FR or NR, no metric is highly consistent with machine preference, although they are all good at predicting human preference. An interesting finding is that **the more accurately and completely a method models the HVS, the more difficult it is to evaluate the perceptual quality of MVS**. Considering that most of the current IQA works emphasize human vision, while machines have already surpassed humans to become the main consumer of visual signals, future IQA needs to find a way to balance these two goals.

For the two distortion subsets, fitting-based methods such as AHIQ/ARNIQA/HyperIQA can achieve SRCC/PLCC values exceeding 0.8 on Severe Distortion. However, this is not a challenging task. Under the same distortion conditions, they have even exceeded 0.95 on the HVS dataset [33, 61]. The performance of Mild Distortion is even worse, and **no method can even outperform the**

Table 3. Cross validation between human and machine preference database. For IQA metrics, **training on machine preference data** can reach a good result in evaluating human preference; but **training on human preference** is unacceptable for MPD. [Keys: **Best**; **Lower** than 0.4.]

Val-set	KADID-10K		TID2013		MPD (Mild)		MPD (Severe)	
	SRCC $\uparrow$	PLCC $\uparrow$						
AHIQ[33]	0.7950	<b>0.7732</b>	0.7651	<b>0.7884</b>	0.1514	0.1846	0.4753	0.3518
CKDN[95]	<b>0.8599</b>	0.7282	0.6989	0.6029	<b>0.1713</b>	<b>0.2055</b>	<b>0.3494</b>	<b>0.3228</b>
DISTS[15]	0.8239	0.8190	0.7231	0.7759	0.4105	0.4077	0.4616	0.4486
LPIS[87]	0.6184	0.5451	0.7054	0.6326	<b>0.2391</b>	<b>0.3118</b>	0.4683	<b>0.3711</b>
PieAPP[62]	0.4783	<b>0.3468</b>	0.6832	0.4543	<b>0.1285</b>	<b>0.0678</b>	<b>0.1791</b>	<b>0.1235</b>
TOPIQ-FR[9]	0.6768	0.6844	<b>0.7782</b>	0.7473	<b>0.5112</b>	<b>0.5495</b>	<b>0.6223</b>	<b>0.6685</b>
ARNIQA[3]	0.7684	0.7023	0.7701	0.7205	0.4829	0.4582	0.5597	0.4849
CLIPQA[62]	0.6286	0.5729	0.5237	<b>0.3910</b>	<b>0.1367</b>	<b>0.1478</b>	<b>0.3201</b>	<b>0.3203</b>
DBCNN[88]	0.5175	0.5351	0.4486	0.5786	<b>0.1359</b>	<b>0.1592</b>	0.4024	<b>0.3877</b>
HyperQA[68]	0.6650	0.6547	0.7024	0.7313	<b>0.0820</b>	<b>0.1074</b>	0.4519	0.4521
NIMA[69]	0.4795	0.4915	0.5694	0.6423	<b>0.1629</b>	<b>0.1775</b>	0.4709	0.4845
TOPIQ-NR[9]	0.5232	0.5077	0.5455	0.6174	<b>0.2388</b>	<b>0.2754</b>	0.4829	0.4582

**simple PSNR, which proves that there is still a lot of room for optimization of IQA for machine preference.**

For the three contents, after verifying them separately, the performance has slightly increased, which is caused by the internal quality differences of the contents. In general, predicting NSI quality is relatively simple, while SCI and AIGI are more difficult. This may be due to the fact that the initial weights of the IQA model have rich NSI priors. For the five dimensions, we can see that the results of MCQ and CAP are most consistent with machine preference; YoN and Others (three common CV tasks) are second; VQA is the worst. This is because VQA problems are usually changes in image details (such as the color of a button on a piece of clothing), which are more difficult for machines to detect than other tasks. In short, IQA for Machine preference still has great research potential, and it is necessary to develop more accurate and effective evaluation mechanisms in the future.

### 5.3. Cross Database Validation

To further analyze the differences between MVS and HVS, we conducted cross-validation using MPD and two of the most commonly used human-oriented datasets, TID2013 [61] and KADID-10K [47], employing the same training mechanism as in the previous chapter. We observed that after training on MPD, most IQA metrics still possess a certain ability to predict human preferences, with SRCC values around 0.7 to 0.8; conversely, after training on the other two human-centric databases, IQA metrics struggle to predict machine preferences, with results on MPD not even reaching 0.4. **Machine preference data will not affect human tasks, but the opposite will.** This finding holds certain guiding significance for future IQA, particularly for a human-machine-friendly paradigm.

### 5.4. Long-term Availability Validation

The machine subjects in MPD are categorized into two groups: common CV models and LMMs. The former mod-

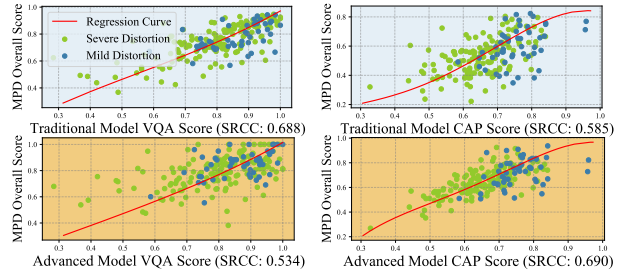


Figure 7. The long-term usability of MPD. The preference scores of MPD are consistent with four early-stage LMMs and three advanced LMMs (marked as **Traditional/Advanced** Models in the background). Their high SRCC proves that MPD can still characterize the perceptual quality of LMMs in the near future.

els, such as the separation/detection benchmark method, have been largely finalized and generally recognized. In contrast, LMMs are still under rapid evolution. It is conceivable that MPD may not be able to capture the LMMs that will emerge in the future, or with the update of MPD, the preference of previous LMMs may be sacrificed. Thus, we include 3 advanced and 4 early-stage LMMs as Sec 3.3 listed, integrating them into two databases similar to MPD. Given the inconsistencies in LMM preference on VQA and CAP tasks, as illustrated in Figure 6, we have verified the consistency of MPD ground truth labels with advanced/early-stage labels. For each image, the relationship between these two labels is depicted in Figure 7. The findings indicate that MPD exhibits a high correlation with early models on VQA and with advanced models on CAP. Generally, the SRCC is around 0.6, which is considered acceptable. Considering the GPT-4o surpasses open-source models, we anticipate that MPD is able to characterize LMMs preferences for images for at least a year. In the future, We will continue to update MPD by periodicity introducing the latest LMMs to avoid this limitation.

## 6. Conclusion

This paper extends the application of IQA from human to machine vision for the first time and establishes the first large-scale, fine-grained, multi-dimensional quality database for machines, namely MPD. We select 15 LMMs and 15 common CV models as subjects, show them 30k reference/distorted image pairs, and summarize their performance on 7 downstream tasks as quality scores. In-depth analysis of the MPD content and IQA benchmark experiments have proved the huge gap between machine and human visual systems, and current human-centric IQA methods cannot accurately predict machine preferences. As the visual data consumption volume of machines has already surpassed humans, we hope that MPD can inspire effective IQA metrics to serve the upcoming machine-centric era.

# Image Quality Assessment: From Human to Machine Preference

## Supplementary Material

### A. Limitation and Broader Impact

**[Limitation 1]:** The main limitation of this study lies in the rapid iteration of LMMs. The study of human-centric IQA is easier because the preferences of different humans do not vary greatly and do not change rapidly over time. The definition of ‘beauty’ in human society typically iterates over centuries. However, mainstream LMMs may be updated annually, and their preferences will also change accordingly. Given that machines are already the primary consumers of visual data, this issue must be addressed. As mentioned in the main text, we can ensure that the annotated data of MPD and the LMMs within a year are relatively consistent. For future LMMs, we will continue to update the machine subjects to ensure their long-term usability of MPD.

**[Limitation 2]:** The calculation method of MOS is also one of the limitations of this study. To comprehensively consider the preferences of machines, we consider seven tasks simultaneously and directly sum  $YoN + MCQ + VQA + CAP + Others$  to derive MOS scores. However, in practical applications, their importance is not necessarily the same, and developers may only focus on certain tasks. In response, we will make the scores of each sub-dimension public, allowing developers to define weights freely. For example, an image compression method aimed at image captioning could increase its share in MOS by only focusing on the *CAP* dimension during training. Thus, the broad applicability of MPD can be guaranteed. (However, the selection of weights still requires manual adjustment.)

**[Broader Impact]:** For the field of IQA, this study has fundamentally overturned the human-centric paradigm that has dominated the past 20 years. MPD has for the first time clearly defined the tasks of ‘IQA for Machine Vision.’ We believe it will inspire future machine-centric IQA methods. For the entire machine vision research community, this study has ended the situation where different models are being operated and evaluated independently. With the vigorous development of machine-oriented image processing algorithms (such as the rapid development of image/video coding for machines in the past five years), MPD unifies its evaluation criteria. Unlike the previous situation where one side used segmentation and the other used detection, MPD makes a fair, broad, and credible evaluation possible. Considering the important position of machines in the consumer terminal, MPD provides direction for its evolution.

### B. Human Expert Labeling

Seven experts with experience in LMM research project participated in the annotation, targeting 1,000 high-quality

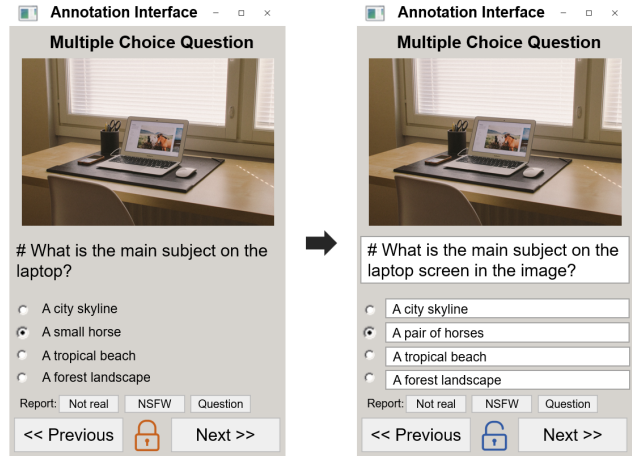


Figure 8. Human annotation interface for YoN/MCQ/VQA tasks. Taking MCQ as an example, viewers can answer directly (left) or modify question/choice (right).

reference images in MPD. Figure 8 shows the user annotation interface, where subjects will complete interspersed YoN/MCQ/VQA/CAP tasks. Taking MCQ as an example, subjects can make the following decisions:

- If they agree with the question design, answer directly and click *Next*;
- If they find some choice is unclear, click *Unlock* to get permission to re-edit the content;
- If they find the question is unclear or too easy, click *Question* after *Unlock*. They may re-design the question-answer pairs and another expert will review whether it is qualified;
- If they find the image is *unnatural* or *NSFW*, click the corresponding button to exclude it.

The principle of YoN/MCQ/VQA question design is to ask about certain aspects of images as detailed as possible. Do not ask a general question like *What does the image show?*, as this is no different from the *CAP* task. For the MCQ task, the three incorrect options need to be as long as the correct option and have the same part of speech to ensure challenge. The expected output for YoN and MCQ is an option (for human experts) and the probability of each option (for LMMs). The expected output for VQA is a short phrase less than 5 words, and for CAP it is a text description of 30-40 words. There is no human involvement in the SEG and DET tasks. In particular, the retrieval range for the RET task is 1,000 category labels generated by GPT-4o, those labels have been double-checked by human experts, thus ensuring the reliability of the proposed MPD.

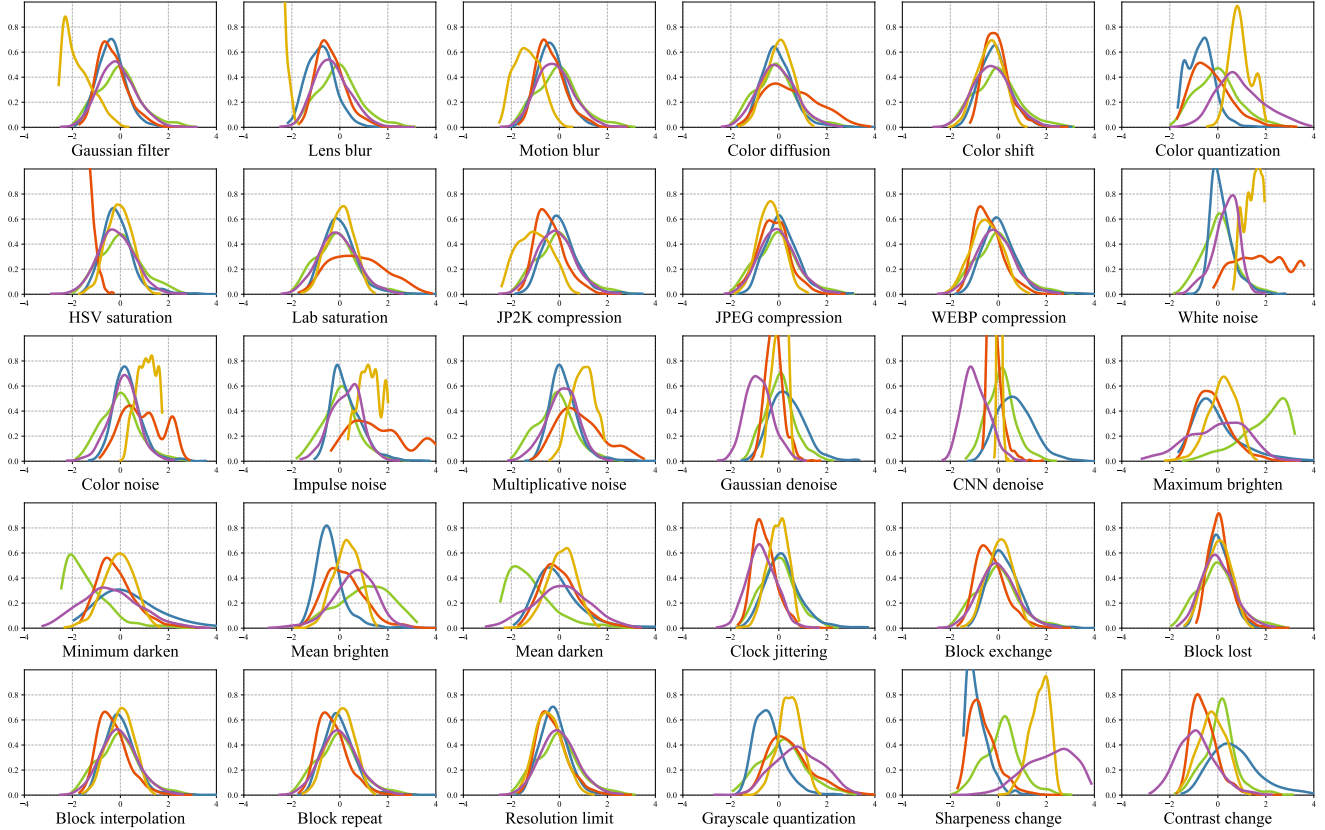


Figure 9. Low-level feature distribution of MPD, normalized and visualized in 30 corruption subsets. Different colors denote **Luminance**, **Contrast**, **Chrominance**, **Blur**, and **Spatial Information**.

## C. Image Feature Distribution

Figure 9 shows the distribution of low-level features of all instances of MPD. After overall regularization, 30 types of corruption are grouped and displayed. The features considered include Luminance, Contrast, Chrominance, Blur, and Spatial Information, and their calculation methods can be found in [35]. There are significant differences in these low-level attributes for different corruptions. For example, in the first three blurry cases, the blur curve is left-biased and becomes right-biased after sharpening. In general, similar corruption categories will lead to similar results (such as five noise-related and four block-related). Two of the denoises have the sharpest distributions; Color quantization, Grayscale quantization, Sharpness change, and Contrast change are the most irregular. These findings deserve further exploration.

## D. Corruption Level

### D.1. Mild&Severe Distortion Split

Due to the different perception mechanisms of MVS and HVS, it is unreasonable to directly regard Strength 1 as

mild, because the machine may be very sensitive to a certain distortion but very robust to another. Therefore, we measured the MPD scores of 30 corruptions and 5 strengths, as shown in Table 4. Overall, as the strength increases, the MOS given by the machine gradually decreases; at the same time, there are huge differences in each corruption itself, which confirms the previous point of view that each corruption needs to be considered separately when dividing. Here, we use 3.333 as the threshold and select a part as the mild validation set in the main text. The specific definition of each corruption is explained in Table 4 as a reference.

### D.2. IQA Evaluation on Different Strength

Table 5 simply shows the performance of IQA algorithms at different Strength levels. Relatively, the performance of ARNIQA and HyperIQA is more satisfactory. However, as shown in each column of Table 4, there are huge differences in machine preferences under the same Strength. Therefore, this is not a challenging task. The performance of the IQA model can only be truly reflected by the MVS-based division in the section D.1, rather than the HVS-based division here.

Table 4. The definition of all 30 corruptions, and their 5 strength level. For each level, the machine preference score in MPD is shown as mean (std). The validation set is split as **Mild** and Severe distortion.

Corruption	Strength 1	Strength 2	Strength 3	Strength 4	Strength 5	Definition
01: Gaussian filter	<b>3.424 (0.203)</b>	3.265 (0.201)	3.112 (0.233)	2.984 (0.255)	2.812 (0.284)	Filter with a variable Gaussian kernel
02: Lens blur	2.857 (0.296)	2.779 (0.318)	2.363 (0.313)	1.999 (0.338)	1.685 (0.254)	Filter with a circular kernel
03: Motion blur	3.300 (0.225)	3.074 (0.266)	2.893 (0.315)	2.738 (0.321)	2.488 (0.346)	Filter with a line kernel
04: Color diffusion	<b>3.571 (0.204)</b>	<b>3.464 (0.190)</b>	<b>3.374 (0.214)</b>	3.299 (0.222)	3.197 (0.242)	Gaussian blur the color channels in the Lab color-space
05: Color shift	3.144 (0.248)	3.116 (0.230)	3.118 (0.260)	3.087 (0.250)	3.115 (0.248)	Randomly translate the green channel
06: Color quantization	3.207 (0.260)	3.055 (0.284)	2.904 (0.276)	2.807 (0.300)	2.503 (0.347)	Using minimum variance quantization in limited color
07: HSV saturation	2.989 (0.367)	2.975 (0.351)	2.933 (0.341)	2.973 (0.334)	2.946 (0.357)	Multiply the saturation channel in the HSV color-space
08: Lab saturation	<b>4.501 (0.232)</b>	<b>3.673 (0.180)</b>	<b>3.480 (0.229)</b>	<b>3.376 (0.220)</b>	3.311 (0.259)	Multiply the saturation channel in the Lab color-space
09: JP2K compression	3.166 (0.269)	2.942 (0.303)	2.831 (0.301)	2.588 (0.377)	2.441 (0.367)	A standard image codec
10: JPEG compression	2.875 (0.269)	2.600 (0.313)	2.446 (0.291)	2.427 (0.269)	2.402 (0.304)	The most widely used image codec
11: WEBP compression	3.053 (0.231)	3.034 (0.231)	3.052 (0.239)	2.985 (0.239)	2.918 (0.267)	Codec with the best comprehensive performance
12: White noise	3.056 (0.242)	2.842 (0.243)	2.666 (0.277)	2.423 (0.325)	2.106 (0.332)	Gaussian white noise to RGB channels
13: Color noise	3.255 (0.207)	3.074 (0.232)	2.938 (0.248)	2.760 (0.267)	2.457 (0.329)	Gaussian white noise to the YCbCr converted image
14: Impulse noise	3.193 (0.214)	3.077 (0.232)	2.911 (0.245)	2.650 (0.283)	2.120 (0.322)	Salt and pepper noise to RGB channels
15: Multiplicative noise	<b>3.368 (0.228)</b>	3.176 (0.246)	3.034 (0.259)	2.894 (0.266)	2.617 (0.293)	Speckle noise to RGB channels
16: Gaussian denoise	2.807 (0.284)	2.655 (0.316)	2.602 (0.275)	2.445 (0.342)	2.345 (0.329)	New noise introduced by Gaussian filter denoise
17: CNN denoise	2.740 (0.292)	2.586 (0.278)	2.514 (0.298)	2.403 (0.338)	2.286 (0.321)	AI-artifacts introduced by neural network denoise
18: Maximum brighten	<b>3.395 (0.193)</b>	3.152 (0.297)	2.964 (0.278)	2.782 (0.309)	2.610 (0.360)	Keep the maximum pixel value and increase others
19: Minimum darken	<b>3.522 (0.193)</b>	3.251 (0.275)	3.018 (0.283)	2.706 (0.374)	2.485 (0.398)	Keep the minimum pixel value and increase others
20: Mean brighten	<b>3.610 (0.216)</b>	<b>3.482 (0.243)</b>	<b>3.370 (0.271)</b>	3.204 (0.258)	3.057 (0.294)	Increase all pixel values and truncate to the original range
21: Mean darken	<b>3.338 (0.274)</b>	3.192 (0.307)	3.024 (0.363)	2.860 (0.369)	2.687 (0.385)	Decrease all pixel values and truncate to the original range
22: Clock jittering	<b>3.472 (0.240)</b>	3.102 (0.301)	2.796 (0.311)	2.472 (0.376)	2.064 (0.383)	Warping each pixel with random small offsets
23: Block exchange	3.161 (0.237)	3.083 (0.216)	2.958 (0.204)	2.874 (0.209)	2.729 (0.223)	The order of two Blocks is wrong
24: Block lost	3.248 (0.223)	3.193 (0.208)	3.091 (0.194)	2.993 (0.193)	2.880 (0.198)	A Block is lost and turned into random pixels
25: Block interpolation	<b>3.547 (0.202)</b>	<b>3.473 (0.202)</b>	<b>3.379 (0.188)</b>	3.290 (0.187)	3.213 (0.193)	A Block is lost and recovered by surrounding pixels
26: Block repeat	<b>3.605 (0.219)</b>	<b>3.554 (0.217)</b>	<b>3.433 (0.236)</b>	<b>3.388 (0.226)</b>	3.228 (0.244)	A Block is convoluted twice on the original position
27: Resolution limit	3.328 (0.242)	3.108 (0.290)	2.784 (0.325)	2.562 (0.344)	2.359 (0.344)	Downsize the image and upsize it back
28: Grayscale quantization	3.332 (0.252)	3.248 (0.269)	3.148 (0.246)	3.008 (0.306)	2.840 (0.281)	Quantize image values using Otsu thresholds
29: Sharpness change	3.110 (0.218)	2.909 (0.250)	2.763 (0.255)	2.589 (0.287)	2.492 (0.306)	Over-sharpen image using unsharp masking
30: Contrast change	<b>3.703 (0.171)</b>	<b>3.606 (0.184)</b>	3.258 (0.221)	3.159 (0.248)	3.037 (0.291)	Non-linearly change RGB values by Sigmoid

Table 5. Using IQA metrics to predict machine preference, including baseline, FR, and NR algorithm, human visual system-based metrics are marked in  $\checkmark$ . The first row represents two distortion intensities and three image content subsets, and the second row represents five scoring dimensions. [Keys: **Best**; **Second best**; **Baseline (BL)**; **Inferior** to the baseline.]

Type	Metric	HVS	Strength 1			Strength 2			Strength 3			Strength 4			Strength 5		
			SRCC $\uparrow$	KRCC $\uparrow$	PLCC $\uparrow$	SRCC $\uparrow$	KRCC $\uparrow$	PLCC $\uparrow$	SRCC $\uparrow$	KRCC $\uparrow$	PLCC $\uparrow$	SRCC $\uparrow$	KRCC $\uparrow$	PLCC $\uparrow$	SRCC $\uparrow$	KRCC $\uparrow$	PLCC $\uparrow$
BL	PSNR		0.3348	0.2400	<b>0.6169</b>	0.2269	0.1497	0.2450	0.2900	0.1958	0.3275	0.2584	0.1733	0.2632	0.3140	0.2115	0.3406
	SSIM		<b>0.5455</b>	<b>0.3720</b>	0.4569	<b>0.5176</b>	<b>0.3571</b>	<b>0.4926</b>	<b>0.4963</b>	<b>0.3395</b>	<b>0.4423</b>	<b>0.4515</b>	<b>0.3058</b>	<b>0.4056</b>	<b>0.5708</b>	<b>0.4008</b>	<b>0.5507</b>
FR	AHIQ		0.6410	0.4625	0.6130	0.7514	0.5639	0.7986	<b>0.7618</b>	<b>0.5793</b>	<b>0.7820</b>	0.7262	0.5340	0.7273	<b>0.8533</b>	<b>0.6721</b>	<b>0.8760</b>
	CKDN	$\checkmark$	0.5770	0.4030	0.4431	0.5966	0.4256	0.5923	0.6285	0.4406	0.6165	0.6347	0.4285	0.5953	0.7538	0.5290	0.7472
	DISTS		0.6813	0.4856	0.6576	0.7013	0.5183	0.7254	0.6569	0.4810	0.6520	0.6471	0.4489	0.6411	0.8324	0.6481	0.8227
	LPIPS	$\checkmark$	0.5238	0.3544	0.3762	0.6266	0.4431	0.5600	0.5375	0.3846	0.4647	0.4229	0.2909	0.3853	0.5138	0.3720	0.4716
	PieAPP	$\checkmark$	0.5145	0.1204	0.3484	0.4180	0.0270	0.2031	0.3717	0.1533	0.1943	0.3241	0.0855	0.1411	0.5709	0.2428	0.3458
	TOPIQ-FR	$\checkmark$	0.6237	0.4358	0.6481	0.7066	0.5166	0.7149	0.6827	0.5006	0.6711	0.6658	0.4594	0.6462	0.7804	0.5842	0.7748
NR	ARNIQA		<b>0.7773</b>	<b>0.5424</b>	<b>0.6305</b>	<b>0.8197</b>	<b>0.6240</b>	<b>0.8339</b>	<b>0.7953</b>	<b>0.5927</b>	<b>0.7416</b>	<b>0.7731</b>	<b>0.5664</b>	<b>0.7331</b>	<b>0.8503</b>	0.6449	0.8353
	CLIQQA	$\checkmark$	0.4365	0.2928	0.3682	0.5556	0.3952	0.5918	0.4809	0.3162	0.4560	0.6352	0.4360	0.5570	0.6970	0.5023	0.6234
	DBCNN	$\checkmark$	0.4863	0.3355	0.4736	0.5338	0.3690	0.5566	0.4682	0.3095	0.4633	0.4420	0.2921	0.4226	0.6430	0.4522	0.6315
	HyperIQA		<b>0.7671</b>	<b>0.5678</b>	<b>0.6647</b>	<b>0.8046</b>	<b>0.6097</b>	<b>0.8211</b>	0.7406	0.5566	0.7543	0.7388	0.5469	0.7473	0.8384	<b>0.6569</b>	<b>0.8604</b>
	NIMA		0.5597	0.3972	0.5243	0.7736	0.5776	0.7767	0.7461	0.5532	0.7831	<b>0.7621</b>	<b>0.5697</b>	<b>0.7607</b>	0.8208	0.6351	0.8488
	TOPIQ-NR	$\checkmark$	0.5650	0.3893	0.5566	0.6056	0.4331	0.6326	0.5852	0.4109	0.5894	0.6407	0.4417	0.6213	0.7219	0.4778	0.6801

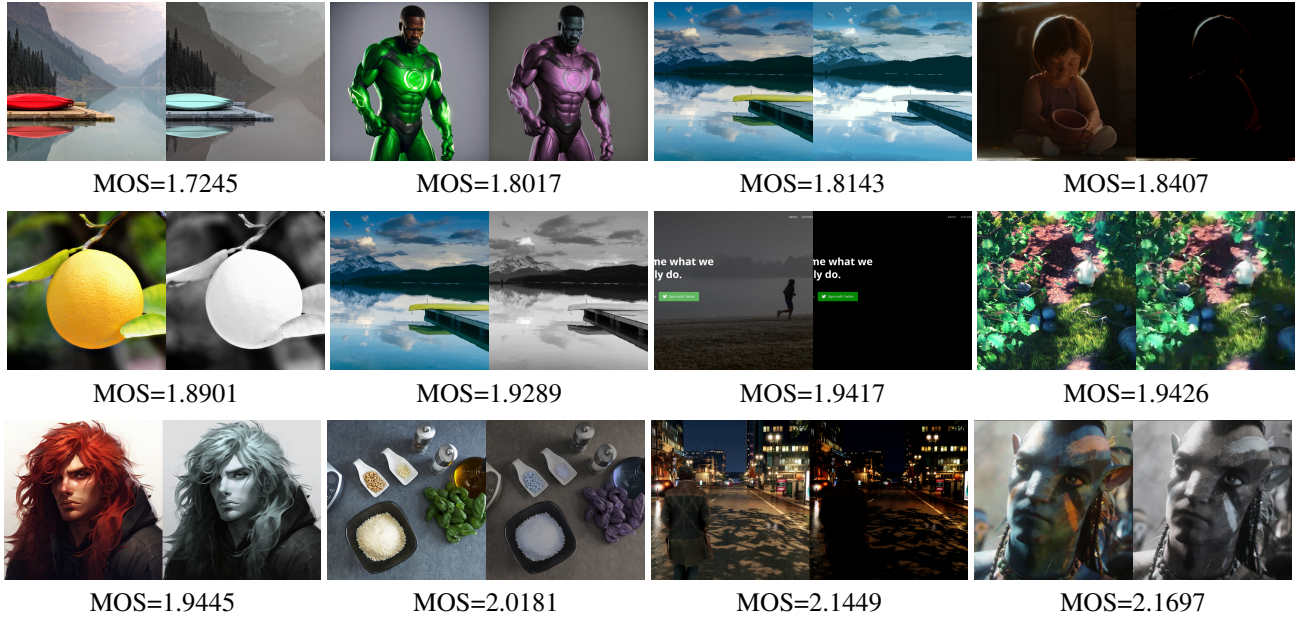


Figure 10. Example of low-quality images for machine preference. (Left: Reference; Right: Distorted, center-cropped as 512×512)

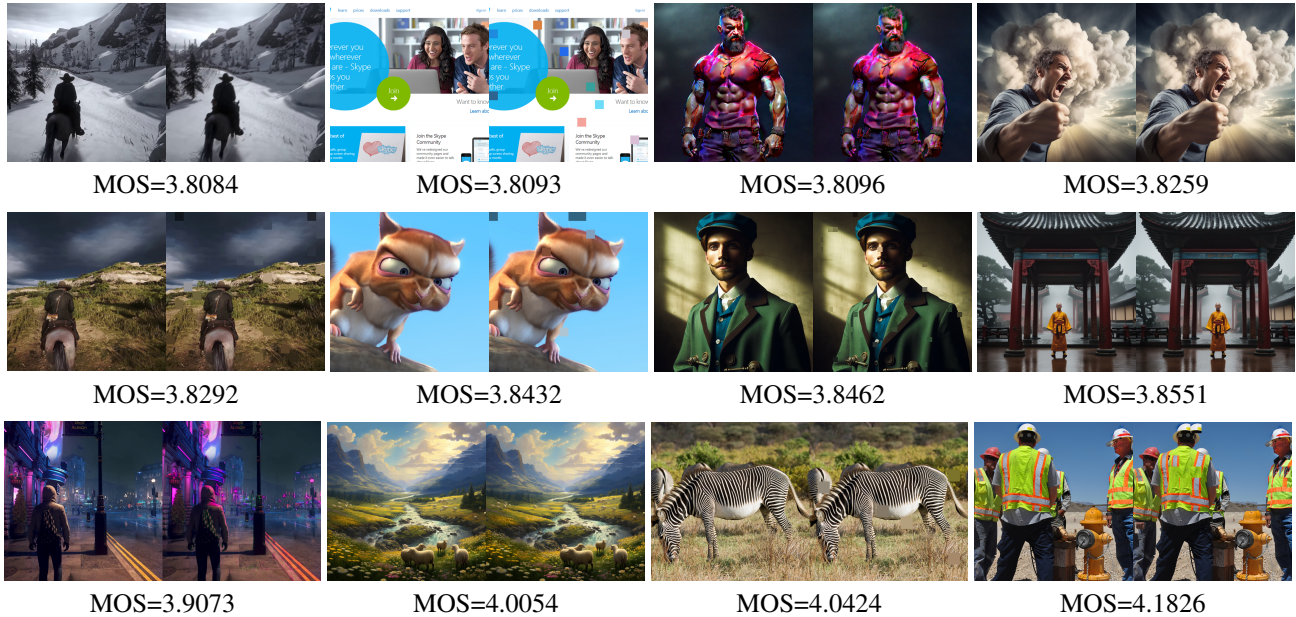


Figure 11. Example of high-quality images for machine preference. (Left: Reference; Right: Distorted, center-cropped as 512×512)

### D.3. Corruption Type&Level Example

Figure 12 shows 30 corruption types at different strength levels from 1 to 5. From a human’s subjective perspective, the visual quality of different corruptions is similar at the same strength. However, from this research, the perception of machines is completely inconsistent. This further proves the huge difference between MVS and HVS.

### E. Example od High&Low Quality Instance

Figures 10 and 11 show low-quality and high-quality examples, with the reference image on the left and the distorted image on the right. Overall, the machine is more robust to pixelation and block-level distortion but has a lower evaluation of grayscale and color changes. We hope that these data from MPD can further reveal the difference between HVS and MVS.

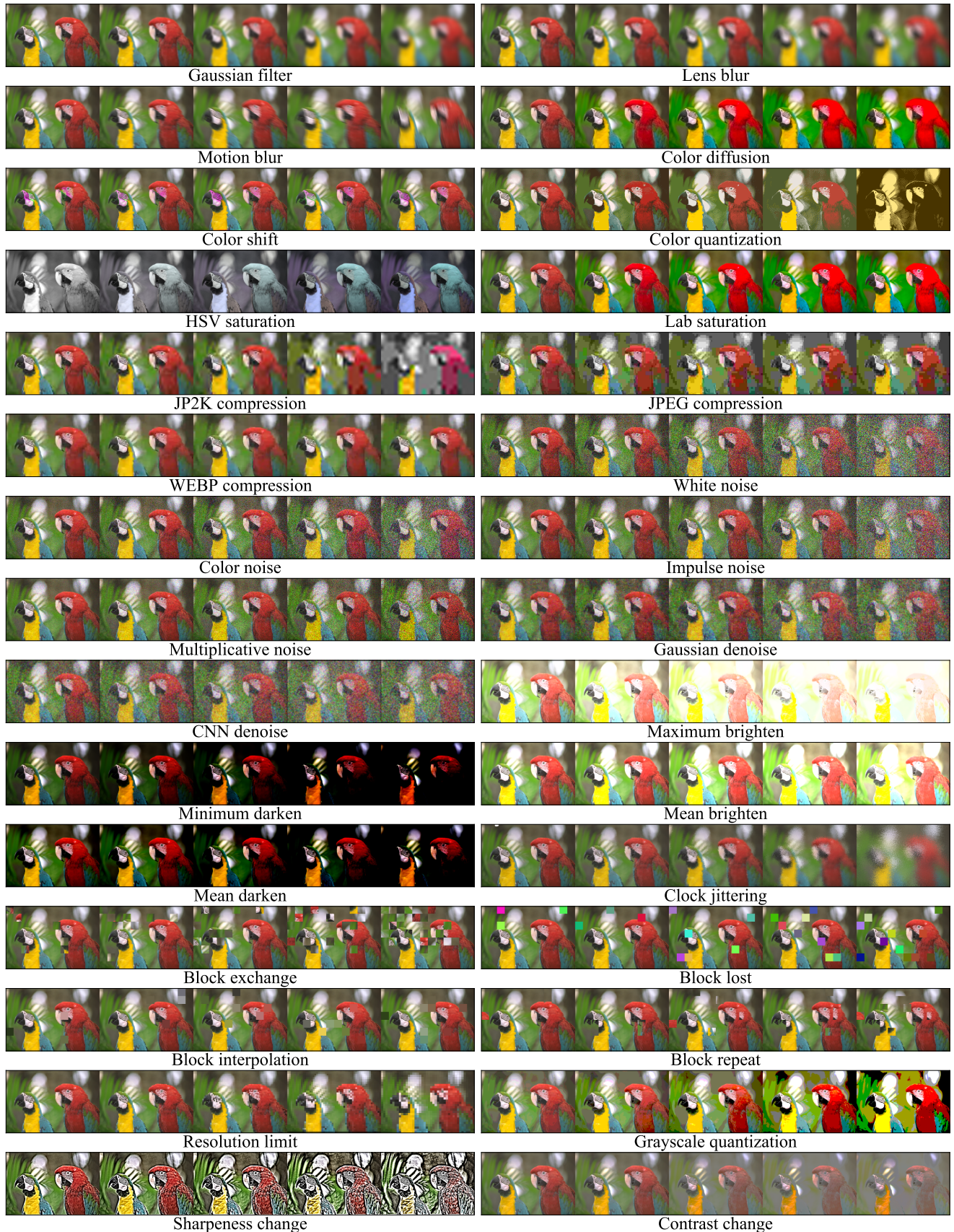


Figure 12. Visualization of 30 types of corruption, zoom in for detail. Strength from left (Level 1) to right (Level 5).

## F. Disclaimer

The main purpose of this study is to propose the technical problem of IQA for Machine Vision, and it does not involve praising or criticizing any IQA models, nor is it a performance basis for IQA. Any IQA metric that performs poorly on MPD does not mean it is inferior. On the contrary, they all have excellent performance in past human-centric IQA while this study is the first machine-centric IQA task. The performance of these state-of-the-art models does not prove a poor capability, but the huge gap in preferences between humans and machines. We will release all data and annotations for non-commercial use, and we sincerely hope that future IQA developers will consider machine preference as an important issue to solve.

## G. Acknowledgment

The work was supported by the National Natural Science Foundation of China under Grant 62225112, 62301310, 623B2073, 62471290; and in part by Sichuan Science and Technology Program under Grant 2024NSFSC1426.

## References

- [1] Marah Abdin, Sam Ade Jacobs, Ammar Ahmad Awan, Jyoti Aneja, Ahmed Awadallah, Hany Awadalla, Nguyen Bach, Amit Bahree, Arash Bakhtiari, Harkirat Behl, et al. Phi-3 technical report: A highly capable language model locally on your phone. *arXiv preprint arXiv:2404.14219*, 2024. 5
- [2] Josh Achiam, Steven Adler, Sandhini Agarwal, Lama Ahmad, Ilge Akkaya, Florencia Leoni Aleman, Diogo Almeida, Janko Altschmidt, Sam Altman, Shyamal Anadkat, et al. Gpt-4 technical report. *arXiv preprint arXiv:2303.08774*, 2023. 5
- [3] Lorenzo Agnolucci, Leonardo Galteri, Marco Bertini, and Alberto Del Bimbo. Arniqa: Learning distortion manifold for image quality assessment. In *2024 IEEE/CVF Winter Conference on Applications of Computer Vision (WACV)*, pages 188–197, 2024. 7, 8
- [4] Peter Anderson, Basura Fernando, Mark Johnson, and Stephen Gould. Spice: Semantic propositional image caption evaluation. In *Computer Vision—ECCV 2016: 14th European Conference, Amsterdam, The Netherlands, October 11–14, 2016, Proceedings, Part V 14*, pages 382–398. Springer, 2016. 4
- [5] Jinze Bai, Shuai Bai, Shusheng Yang, Shijie Wang, Sinan Tan, Peng Wang, Junyang Lin, Chang Zhou, and Jingren Zhou. Qwen-vl: A frontier large vision-language model with versatile abilities. *arXiv preprint arXiv:2308.12966*, 2023. 5
- [6] Johannes Ballé, Philip A Chou, David Minnen, Saurabh Singh, Nick Johnston, Eirikur Agustsson, Sung Jin Hwang, and George Toderici. Nonlinear transform coding. *IEEE Journal of Selected Topics in Signal Processing*, 15(2):339–353, 2020. 2, 3
- [7] Min Cao, Shiping Li, Juntao Li, Liqiang Nie, and Min Zhang. Image-text retrieval: A survey on recent research and development. In *Proceedings of the Thirty-First International Joint Conference on Artificial Intelligence, IJCAI-22*, pages 5410–5417. International Joint Conferences on Artificial Intelligence Organization, 2022. Survey Track. 4
- [8] Junsong Chen, Jincheng Yu, Chongjian Ge, Lewei Yao, Enze Xie, Yue Wu, Zhongdao Wang, James Kwok, Ping Luo, Huchuan Lu, and Zhenguo Li. Pixart- $\alpha$ : Fast training of diffusion transformer for photorealistic text-to-image synthesis, 2023. 3
- [9] Chaofeng Chen, Jiadi Mo, Jingwen Hou, Haoning Wu, Liang Liao, Wenxiu Sun, Qiong Yan, and Weisi Lin. Topiq: A top-down approach from semantics to distortions for image quality assessment. *IEEE Transactions on Image Processing*, 33:2404–2418, 2024. 7, 8
- [10] Zhe Chen, Weiyun Wang, Hao Tian, Shenglong Ye, Zhangwei Gao, Erfei Cui, Wenwen Tong, Kongzhi Hu, Jiapeng Luo, Zheng Ma, et al. How far are we to gpt-4v? closing the gap to commercial multimodal models with open-source suites. *arXiv preprint arXiv:2404.16821*, 2024. 5
- [11] Zhe Chen, Jiannan Wu, Wenhai Wang, Weijie Su, Guo Chen, Sen Xing, Muyan Zhong, Qinglong Zhang, Xizhou Zhu, Lewei Lu, Bin Li, Ping Luo, Tong Lu, Yu Qiao, and Jifeng Dai. Internvl: Scaling up vision foundation models and aligning for generic visual-linguistic tasks. In *Proceedings of the IEEE/CVF Conference on Computer Vision and Pattern Recognition (CVPR)*, pages 24185–24198, 2024. 5
- [12] Jinyoung Choi and Bohyung Han. Task-aware quantization network for jpeg image compression. In *Computer Vision—ECCV 2020: 16th European Conference, Glasgow, UK, August 23–28, 2020, Proceedings, Part XX 16*, pages 309–324. Springer, 2020. 3
- [13] U Cisco. Cisco annual internet report (2018–2023) white paper. *Cisco: San Jose, CA, USA*, 10(1):1–35, 2020. 1
- [14] Wenliang Dai, Junnan Li, Dongxu Li, Anthony Meng Huat Tiong, Junqi Zhao, Weisheng Wang, Boyang Li, Pascale Fung, and Steven Hoi. Instructblip: Towards general-purpose vision-language models with instruction tuning, 2023. 5
- [15] Keyan Ding, Kede Ma, Shiqi Wang, and Eero P Simoncelli. Image quality assessment: Unifying structure and texture similarity. *IEEE transactions on pattern analysis and machine intelligence*, 44(5):2567–2581, 2020. 7, 8
- [16] Xiaoyi Dong, Pan Zhang, Yuhang Zang, Yuhang Cao, Bin Wang, Linke Ouyang, Xilin Wei, Songyang Zhang, Haodong Duan, Maosong Cao, Wenwei Zhang, Yining Li, Hang Yan, Yang Gao, Xinyue Zhang, Wei Li, Jingwen Li, Kai Chen, Conghui He, Xingcheng Zhang, Yu Qiao, Dahua Lin, and Jiaqi Wang. Internlm-xcomposer2: Mastering free-form text-image composition and comprehension in vision-language large model. *arXiv preprint arXiv:2401.16420*, 2024. 5
- [17] Zhengxiao Du, Yujie Qian, Xiao Liu, Ming Ding, Jiezhong Qiu, Zhilin Yang, and Jie Tang. Glm: General language model pretraining with autoregressive blank infilling. In *Proceedings of the 60th Annual Meeting of the Association for Computational Linguistics (Volume 1: Long Papers)*, pages 320–335, 2022. 5
- [18] Haodong Duan, Junming Yang, Yuxuan Qiao, Xinyu Fang, Lin Chen, Yuan Liu, Xiaoyi Dong, Yuhang Zang, Pan Zhang,

- Jiaqi Wang, Dahua Lin, and Kai Chen. Vlmevalkit: An open-source toolkit for evaluating large multi-modality models, 2024. 4
- [19] Fartash Faghri, David J Fleet, Jamie Ryan Kiros, and Sanja Fidler. Vse++: Improving visual-semantic embeddings with hard negatives. *arXiv preprint arXiv:1707.05612*, 2017. 5
- [20] Wen Gao, Siwei Ma, Lingyu Duan, Yonghong Tian, Peiyin Xing, Yaowei Wang, Shanshe Wang, Huizhu Jia, and Tiejun Huang. Digital retina: A way to make the city brain more efficient by visual coding. *IEEE Transactions on Circuits and Systems for Video Technology*, 31(11):4147–4161, 2021. 1
- [21] Yixuan Gao, Yuqin Cao, Tengchuan Kou, Wei Sun, Yunlong Dong, Xiaohong Liu, Xiongkuo Min, and Guangtao Zhai. Vdpe: Vqa dataset for perceptual video enhancement. In *Proceedings of the IEEE/CVF Conference on Computer Vision and Pattern Recognition (CVPR) Workshops*, pages 1474–1483, 2023. 2
- [22] Zhangwei Gao, Zhe Chen, Erfei Cui, Yiming Ren, Weiyun Wang, Jinguo Zhu, Hao Tian, Shenglong Ye, Junjun He, Xizhou Zhu, Lewei Lu, Tong Lu, Yu Qiao, Jifeng Dai, and Wenhui Wang. Mini-intervnl: A flexible-transfer pocket multimodal model with 55
- [23] Zheng Ge, Songtao Liu, Feng Wang, Zeming Li, and Jian Sun. YOLOX: Exceeding yolo series in 2021. *arXiv preprint arXiv:2107.08430*, 2021. 5
- [24] Jinjin Gu, Haoming Cai, Chao Dong, Jimmy S Ren, Radu Timofte, Yuan Gong, Shanshan Lao, Shuwei Shi, Jiahao Wang, Sidi Yang, et al. Ntire 2022 challenge on perceptual image quality assessment. In *Proceedings of the IEEE/CVF conference on computer vision and pattern recognition*, pages 951–967, 2022. 2
- [25] Yatharth Gupta, Vishnu V. Jaddipal, Harish Prabhala, Sayak Paul, and Patrick Von Platen. Progressive knowledge distillation of stable diffusion xl using layer level loss, 2024. 3
- [26] Shijie Hao, Yuan Zhou, and Yanrong Guo. A brief survey on semantic segmentation with deep learning. *Neurocomputing*, 406:302–321, 2020. 4
- [27] Kaiming He, Georgia Gkioxari, Piotr Dollar, and Ross Girshick. Mask r-cnn. *2017 IEEE International Conference on Computer Vision (ICCV)*, 2017. 5
- [28] David Holz. Midjourney. <https://www.midjourney.com>, 2023. 3
- [29] Vlad Hosu, Hanhe Lin, Tamas Sziranyi, and Dietmar Saupé. Koniq-10k: An ecologically valid database for deep learning of blind image quality assessment. *IEEE Transactions on Image Processing*, 29:4041–4056, 2020. 2
- [30] Yunzhong Hou, Liang Zheng, and Stephen Gould. Learning to structure an image with few colors. In *Proceedings of the IEEE/cvf conference on computer vision and pattern recognition*, pages 10116–10125, 2020. 3
- [31] Zhimeng Huang, Chuanmin Jia, Shanshe Wang, and Siwei Ma. Visual analysis motivated rate-distortion model for image coding. In *2021 IEEE International Conference on Multimedia and Expo (ICME)*, pages 1–6. IEEE, 2021. 3
- [32] Dongfu Jiang, Xuan He, Huaye Zeng, Cong Wei, Max Ku, Qian Liu, and Wenhui Chen. Mantis: Interleaved multi-image instruction tuning, 2024. 5
- [33] Shanshan Lao, Yuan Gong, Shuwei Shi, Sidi Yang, Tianhe Wu, Jiahao Wang, Weihao Xia, and Yujiu Yang. Attentions help cnns see better: Attention-based hybrid image quality assessment network, 2022. 7, 8
- [34] Yanghao Li, Hanzi Mao, Ross Girshick, and Kaiming He. Exploring plain vision transformer backbones for object detection. In *European conference on computer vision*, pages 280–296. Springer, 2022. 3, 5
- [35] Chunyi Li, Zicheng Zhang, Haoning Wu, Wei Sun, Xiongkuo Min, Xiaohong Liu, Guangtao Zhai, and Weisi Lin. Aigqa-3k: An open database for ai-generated image quality assessment. *IEEE Transactions on Circuits and Systems for Video Technology*, 2023. 2, 10
- [36] Junnan Li, Dongxu Li, Silvio Savarese, and Steven Hoi. Blip-2: Bootstrapping language-image pre-training with frozen image encoders and large language models. In *International conference on machine learning*, pages 19730–19742. PMLR, 2023. 5
- [37] Bo Li, Yuanhan Zhang, Dong Guo, Renrui Zhang, Feng Li, Hao Zhang, Kaichen Zhang, Yanwei Li, Ziwei Liu, and Chunyuan Li. Llava-onevision: Easy visual task transfer. *arXiv preprint arXiv:2408.03326*, 2024. 5
- [38] Chunyi Li, Tengchuan Kou, Yixuan Gao, Yuqin Cao, Wei Sun, Zicheng Zhang, Yingjie Zhou, Zhichao Zhang, Weixia Zhang, Haoning Wu, Xiaohong Liu, Xiongkuo Min, and Guangtao Zhai. Aigqa-20k: A large database for ai-generated image quality assessment, 2024. 2
- [39] Chunyi Li, Guo Lu, Donghui Feng, Haoning Wu, Zicheng Zhang, Xiaohong Liu, Guangtao Zhai, Weisi Lin, and Wenjun Zhang. Misc: Ultra-low bitrate image semantic compression driven by large multimodal model, 2024. 1
- [40] Chunyi Li, Haoning Wu, Hongkun Hao, Zicheng Zhang, Tengchuan Kou, Chaofeng Chen, Lei Bai, Xiaohong Liu, Weisi Lin, and Guangtao Zhai. G-refine: A general quality refiner for text-to-image generation. In *Proceedings of the 32nd ACM International Conference on Multimedia*, page 7375–7384, New York, NY, USA, 2024. Association for Computing Machinery.
- [41] Chunyi Li, Haoning Wu, Zicheng Zhang, Hongkun Hao, Kaiwei Zhang, Lei Bai, Xiaohong Liu, Xiongkuo Min, Weisi Lin, and Guangtao Zhai. Q-refine: A perceptual quality refiner for ai-generated image. In *2024 IEEE International Conference on Multimedia and Expo (ICME)*, pages 1–6, 2024. 1
- [42] Chunyi Li, Xiele Wu, Haoning Wu, Donghui Feng, Zicheng Zhang, Guo Lu, Xiongkuo Min, Xiaohong Liu, Guangtao Zhai, and Weisi Lin. Cmc-bench: Towards a new paradigm of visual signal compression, 2024. 3
- [43] Daiqing Li, Aleks Kamko, Ehsan Akhgari, Ali Sabet, Linmiao Xu, and Suhail Doshi. Playground v2.5: Three insights towards enhancing aesthetic quality in text-to-image generation, 2024. 3
- [44] Feng Li, Renrui Zhang, Hao Zhang, Yuanhan Zhang, Bo Li, Wei Li, Zejun Ma, and Chunyuan Li. Llava-next-interleave: Tackling multi-image, video, and 3d in large multimodal models. *arXiv preprint arXiv:2407.07895*, 2024. 5
- [45] Zhang Li, Biao Yang, Qiang Liu, Zhiyin Ma, Shuo Zhang, Jingxu Yang, Yabo Sun, Yuliang Liu, and Xiang Bai. Mon-

- key: Image resolution and text label are important things for large multi-modal models. In *proceedings of the IEEE/CVF conference on computer vision and pattern recognition*, 2024. 5
- [46] Tsung-Yi Lin, Michael Maire, Serge Belongie, James Hays, Pietro Perona, Deva Ramanan, Piotr Dollár, and C Lawrence Zitnick. Microsoft coco: Common objects in context. In *Computer Vision–ECCV 2014: 13th European Conference, Zurich, Switzerland, September 6–12, 2014, Proceedings, Part V 13*, pages 740–755. Springer, 2014. 3
- [47] Hanhe Lin, Vlad Hosu, and Dietmar Saupe. Kadid-10k: A large-scale artificially distorted iqa database. In *2019 Tenth International Conference on Quality of Multimedia Experience (QoMEX)*, pages 1–3. IEEE, 2019. 2, 6, 8
- [48] Risheng Liu, Long Ma, Tengyu Ma, Xin Fan, and Zhongxuan Luo. Learning with nested scene modeling and cooperative architecture search for low-light vision. *IEEE Transactions on Pattern Analysis and Machine Intelligence*, 45(5): 5953–5969, 2022. 3
- [49] Haotian Liu, Chunyuan Li, Qingyang Wu, and Yong Jae Lee. Visual instruction tuning. In *Advances in Neural Information Processing Systems*, pages 34892–34916. Curran Associates, Inc., 2023. 5
- [50] Yuan Liu, Haodong Duan, Yuanhan Zhang, Bo Li, Songyang Zhang, Wangbo Zhao, Yike Yuan, Jiaqi Wang, Conghui He, Ziwei Liu, et al. Mmbench: Is your multi-modal model an all-around player? *arXiv preprint arXiv:2307.06281*, 2023. 4
- [51] Xiaohong Liu, Xiongkuo Min, Guangtao Zhai, Chunyi Li, Tengchuan Kou, et al. Ntire 2024 quality assessment of ai-generated content challenge. In *Proceedings of the IEEE/CVF Conference on Computer Vision and Pattern Recognition (CVPR) Workshops*, pages 6337–6362, 2024. 2
- [52] Yuan Liu, Le Tian, Xiao Zhou, and Jie Zhou. Rethinking overlooked aspects in vision-language models. *arXiv preprint arXiv:22405.11850*, 2024. 5
- [53] Haoyu Lu, Wen Liu, Bo Zhang, Bingxuan Wang, Kai Dong, Bo Liu, Jingxiang Sun, Tongzheng Ren, Zhuoshu Li, Yaofeng Sun, et al. Deepseek-vl: towards real-world vision-language understanding. *arXiv preprint arXiv:2403.05525*, 2024. 5
- [54] Shiyin Lu, Yang Li, Qing-Guo Chen, Zhao Xu, Weihua Luo, Kaifu Zhang, and Han-Jia Ye. Ovis: Structural embedding alignment for multimodal large language model, 2024. 5
- [55] Chengqi Lyu, Wenwei Zhang, Haiyan Huang, Yue Zhou, Yudong Wang, Yanyi Liu, Shilong Zhang, and Kai Chen. Rtm-det: An empirical study of designing real-time object detectors. *arXiv preprint arXiv:2212.07784*, 2022. 5
- [56] Xiongkuo Min, Kede Ma, Ke Gu, Guangtao Zhai, Zhou Wang, and Weisi Lin. Unified blind quality assessment of compressed natural, graphic, and screen content images. *IEEE Transactions on Image Processing*, 26(11):5462–5474, 2017. 2, 3
- [57] Anush Krishna Moorthy and Alan Conrad Bovik. Blind image quality assessment: From natural scene statistics to perceptual quality. *IEEE transactions on Image Processing*, 20(12):3350–3364, 2011. 2
- [58] Zhangkai Ni, Lin Ma, Huanqiang Zeng, Jing Chen, Canhui Cai, and Kai-Kuang Ma. Esim: Edge similarity for screen content image quality assessment. *IEEE Transactions on Image Processing*, 26(10):4818–4831, 2017. 2
- [59] Kishore Papineni, Salim Roukos, Todd Ward, and Wei-Jing Zhu. Bleu: a method for automatic evaluation of machine translation. In *Proceedings of the 40th annual meeting of the Association for Computational Linguistics*, pages 311–318, 2002. 4
- [60] Neel Patwa, Nilesh Ahuja, Srinivasa Somayazulu, Omesh Tickoo, Srenivas Varadarajan, and Shashidhar Koolagudi. Semantic-preserving image compression. In *2020 IEEE International Conference on Image Processing (ICIP)*, pages 1281–1285. IEEE, 2020. 3
- [61] Nikolay Ponomarenko, Lina Jin, Oleg Ieremeiev, Vladimir Lukin, Karen Egiazarian, Jaakko Astola, Benoit Vozel, Kacem Chehdi, Marco Carli, Federica Battisti, et al. Image database tid2013: Peculiarities, results and perspectives. *Signal processing: Image communication*, 30:57–77, 2015. 2, 7, 8
- [62] Ekta Prashnani, Hong Cai, Yasamin Mostofi, and Pradeep Sen. Pieapp: Perceptual image-error assessment through pairwise preference. In *Proceedings of the IEEE Conference on Computer Vision and Pattern Recognition*, pages 1808–1817, 2018. 7, 8
- [63] Leigang Qu, Meng Liu, Jianlong Wu, Zan Gao, and Liqiang Nie. Dynamic modality interaction modeling for image-text retrieval. In *Proceedings of the 44th International ACM SIGIR Conference on Research and Development in Information Retrieval*, pages 1104–1113, 2021. 5
- [64] Aditya Ramesh, Prafulla Dhariwal, Alex Nichol, Casey Chu, and Mark Chen. Hierarchical text-conditional image generation with clip latents, 2022. 3
- [65] Shaoqing Ren, Kaiming He, Ross Girshick, and Jian Sun. Faster r-cnn: Towards real-time object detection with region proposal networks. *IEEE Transactions on Pattern Analysis and Machine Intelligence*, 2017. 3, 5
- [66] Robin Rombach, Andreas Blattmann, and Björn Ommer. Text-guided synthesis of artistic images with retrieval-augmented diffusion models, 2022. 3
- [67] Chengyao Shen and Qi Zhao. Webpage saliency. In *Computer Vision–ECCV 2014: 13th European Conference, Zurich, Switzerland, September 6–12, 2014, Proceedings, Part VII 13*, pages 33–46. Springer, 2014. 3
- [68] Shaolin Su, Qingsen Yan, Yu Zhu, Cheng Zhang, Xin Ge, Jinqiu Sun, and Yanning Zhang. Blindly assess image quality in the wild guided by a self-adaptive hyper network. In *Proceedings of the IEEE/CVF Conference on Computer Vision and Pattern Recognition*, pages 3667–3676, 2020. 7, 8
- [69] Hossein Talebi and Peyman Milanfar. Nima: Neural image assessment. *IEEE Transactions on Image Processing*, 27(8): 3998–4011, 2018. 7, 8
- [70] Zhi Tian, Chunhua Shen, Xinlong Wang, and Hao Chen. Boxinst: High-performance instance segmentation with box annotations. In *Proceedings of the IEEE/CVF Conference on Computer Vision and Pattern Recognition*, pages 5443–5452, 2021. 5

- [71] I. T. Union. Methodology for the subjective assessment of the quality of television pictures. *ITU-R Recommendation BT. 500-11*, 2002. 5, 6
- [72] Ramakrishna Vedantam, C Lawrence Zitnick, and Devi Parikh. Cider: Consensus-based image description evaluation. In *Proceedings of the IEEE conference on computer vision and pattern recognition*, pages 4566–4575, 2015. 4
- [73] Thang Vu, Haeyong Kang, and Chang D Yoo. Scnet: Training inference sample consistency for instance segmentation. In *Proceedings of the AAAI Conference on Artificial Intelligence*, pages 2701–2709, 2021. 5
- [74] Jianyi Wang, Kelvin CK Chan, and Chen Change Loy. Exploring clip for assessing the look and feel of images. In *Proceedings of the AAAI Conference on Artificial Intelligence*, pages 2555–2563, 2023. 7
- [75] Peng Wang, Shuai Bai, Sinan Tan, Shijie Wang, Zhihao Fan, Jinze Bai, Keqin Chen, Xuejing Liu, Jialin Wang, Wenbin Ge, et al. Qwen2-vl: Enhancing vision-language model’s perception of the world at any resolution. *arXiv preprint arXiv:2409.12191*, 2024. 5
- [76] Zhou Wang. Image quality assessment: from error visibility to structural similarity. *IEEE transactions on image processing*, 13(4):600–612, 2004. 7
- [77] Sanghyun Woo, Shoubhik Debnath, Ronghang Hu, Xinlei Chen, Zhuang Liu, In So Kweon, and Saining Xie. Convnext v2: Co-designing and scaling convnets with masked autoencoders. In *Proceedings of the IEEE/CVF Conference on Computer Vision and Pattern Recognition*, pages 16133–16142, 2023. 5
- [78] Haoning Wu, Zicheng Zhang, Erli Zhang, Chaofeng Chen, Liang Liao, Annan Wang, Chunyi Li, Wenxiu Sun, Qiong Yan, Guangtao Zhai, et al. Q-bench: A benchmark for general-purpose foundation models on low-level vision. *arXiv preprint arXiv:2309.14181*, 2023. 4
- [79] XAI. grok-1.5v, 2024. 4
- [80] Zhaohui Yang, Yunhe Wang, Chang Xu, Peng Du, Chao Xu, Chunjing Xu, and Qi Tian. Discernible image compression. In *Proceedings of the 28th ACM International Conference on Multimedia*, pages 1561–1569, 2020. 3
- [81] Jiabo Ye, Haiyang Xu, Haowei Liu, Anwen Hu, Ming Yan, Qi Qian, Ji Zhang, Fei Huang, and Jingren Zhou. mplug-owl3: Towards long image-sequence understanding in multi-modal large language models. *arXiv preprint arXiv:2408.04840*, 2024. 5
- [82] Qinghao Ye, Haiyang Xu, Jiabo Ye, Ming Yan, Anwen Hu, Haowei Liu, Qi Qian, Ji Zhang, and Fei Huang. mplug-owl2: Revolutionizing multi-modal large language model with modality collaboration. In *Proceedings of the IEEE/CVF Conference on Computer Vision and Pattern Recognition*, pages 13040–13051, 2024. 5
- [83] Masakazu Yoshimura, Junji Otsuka, Atsushi Irie, and Takeshi Ohashi. Dynamicisp: dynamically controlled image signal processor for image recognition. In *Proceedings of the IEEE/CVF International Conference on Computer Vision*, pages 12866–12876, 2023. 3
- [84] Ke Yu, Zexian Li, Yue Peng, Chen Change Loy, and Jinwei Gu. Reconfigisp: Reconfigurable camera image processing pipeline. In *Proceedings of the IEEE/CVF International Conference on Computer Vision*, pages 4248–4257, 2021. 3
- [85] Xiang Yue, Yueqi Song, Akari Asai, Seungone Kim, Jean de Dieu Nyandwi, Simran Khanuja, Anjali Kantharuban, Lintang Sutawika, Sathyanarayanan Ramamoorthy, and Graham Neubig. Pangea: A fully open multilingual multimodal llm for 39 languages, 2024. 5
- [86] Jing Zhang and Dacheng Tao. Empowering things with intelligence: a survey of the progress, challenges, and opportunities in artificial intelligence of things. *IEEE Internet of Things Journal*, 8(10):7789–7817, 2020. 1
- [87] Richard Zhang, Phillip Isola, Alexei A Efros, Eli Shechtman, and Oliver Wang. The unreasonable effectiveness of deep features as a perceptual metric. In *Proceedings of the IEEE conference on computer vision and pattern recognition*, pages 586–595, 2018. 7, 8
- [88] Weixia Zhang, Kede Ma, Jia Yan, Dexiang Deng, and Zhou Wang. Blind image quality assessment using a deep bilinear convolutional neural network. *IEEE Transactions on Circuits and Systems for Video Technology*, 30(1):36–47, 2018. 7, 8
- [89] Hao Zhang, Feng Li, Shilong Liu, Lei Zhang, Hang Su, Jun Zhu, Lionel M Ni, and Heung-Yeung Shum. Dino: Detr with improved denoising anchor boxes for end-to-end object detection. *arXiv preprint arXiv:2203.03605*, 2022. 5
- [90] Kun Zhang, Zhendong Mao, Quan Wang, and Yongdong Zhang. Negative-aware attention framework for image-text matching. In *Proceedings of the IEEE/CVF conference on computer vision and pattern recognition*, pages 15661–15670, 2022. 5
- [91] Zicheng Zhang, Chunyi Li, Wei Sun, Xiaohong Liu, Xiongkuo Min, and Guangtao Zhai. A perceptual quality assessment exploration for aigc images. In *IEEE International Conference on Multimedia and Expo Workshops (ICMEW)*, pages 440–445, 2023. 2
- [92] Zicheng Zhang, Wei Sun, Yingjie Zhou, Jun Jia, Zhichao Zhang, Jing Liu, Xiongkuo Min, and Guangtao Zhai. Subjective and objective quality assessment for in-the-wild computer graphics images. *ACM Transactions on Multimedia Computing, Communications and Applications*, 20(4):1–22, 2023. 3
- [93] Qi Zhang, Shanshe Wang, Xinfeng Zhang, Chuanmin Jia, Zhao Wang, Siwei Ma, and Wen Gao. Perceptual video coding for machines via satisfied machine ratio modeling, 2024. 2
- [94] Qi Zhang, Shanshe Wang, Xinfeng Zhang, Siwei Ma, Jingshan Pan, and Wen Gao. Predicting satisfied user and machine ratio for compressed images: A unified approach, 2024. 2
- [95] Heliang Zheng, Huan Yang, Jianlong Fu, Zheng-Jun Zha, and Jiebo Luo. Learning conditional knowledge distillation for degraded-reference image quality assessment. In *Proceedings of the IEEE/CVF International Conference on Computer Vision (ICCV)*, pages 10242–10251, 2021. 7, 8
- [96] Zhengxia Zou, Keyan Chen, Zhenwei Shi, Yuhong Guo, and Jieping Ye. Object detection in 20 years: A survey. *Proceedings of the IEEE*, 111(3):257–276, 2023. 4